



Western Michigan University
ScholarWorks at WMU

Masters Theses

Graduate College

12-1991

An Experimental Investigation of Bevelled Blade Coating for Paper

Mustafa Naci Altug
Western Michigan University

Follow this and additional works at: https://scholarworks.wmich.edu/masters_theses



Part of the Materials Science and Engineering Commons

Recommended Citation

Altug, Mustafa Naci, "An Experimental Investigation of Bevelled Blade Coating for Paper" (1991). *Masters Theses*. 948.

https://scholarworks.wmich.edu/masters_theses/948

This Masters Thesis-Open Access is brought to you for free and open access by the Graduate College at ScholarWorks at WMU. It has been accepted for inclusion in Masters Theses by an authorized administrator of ScholarWorks at WMU. For more information, please contact wmu-scholarworks@wmich.edu.



AN EXPERIMENTAL INVESTIGATION OF BEVELLED
BLADE COATING FOR PAPER

by

Mustafa Naci Altug

A Thesis
Submitted to the
Faculty of The Graduate College
in partial fulfillment of the
requirements for the
Degree of Master of Science
Department of Paper and Printing
Science and Engineering

Western Michigan University
Kalamazoo, Michigan
December 1991

AN EXPERIMENTAL INVESTIGATION OF BEVELLED
BLADE COATING FOR PAPER

Mustafa Naci Altug, M.S.

Western Michigan University, 1991

In this study the total dynamic force (TDF) acting on the blade was determined at three different web speeds. The objective was to compare quantitatively the experimental results with the predictions of existing models to show whether or not any of these models predict coat weight development. The existing models include the lubrication theory, impact model, lateral force, and combinations of these models.

Under the conditions investigated, the estimated TDF was in good agreement only with the impact force (sum of impulse and hydrodynamic forces) model of blade coating. The impulse force accounted for 94% of the TDF and, therefore, was considered the dominant contributor to coat weight development. Data suggested that the momentum change of coating layer entering the blade nip region has been counted twice in the original proposed model. If lubrication flow alone was considered at the blade tip, the hydrodynamic lift could contribute maximum 30 to 48% of the TDF. Finally, the recently proposed lateral force at the nip was calculated to be only 6 to 7% of TDF.

ACKNOWLEDGEMENTS

I wish to express a special acknowledgement and sincere appreciation to my committee chairperson, Dr. Nicholas G. Triantafillopoulos, for his assistance, direction, and support; and to my committee members, James E. Kline and Dr. Raymond L. Janes for their advice and guidance.

Appreciation is expressed to the Turkish Government for the financial support during my course of study. Appreciation is also due to Irmak Yayin for his suggestions and constructive criticism.

Finally, my deepest gratitude, thanks, and appreciation are extended to my wife, Zehra, and my daughter, Sila, for their love, support, and encouragement needed to bring this study to completion.

Mustafa Naci Altug

INFORMATION TO USERS

This manuscript has been reproduced from the microfilm master. UMI films the text directly from the original or copy submitted. Thus, some thesis and dissertation copies are in typewriter face, while others may be from any type of computer printer.

The quality of this reproduction is dependent upon the quality of the copy submitted. Broken or indistinct print, colored or poor quality illustrations and photographs, print bleedthrough, substandard margins, and improper alignment can adversely affect reproduction.

In the unlikely event that the author did not send UMI a complete manuscript and there are missing pages, these will be noted. Also, if unauthorized copyright material had to be removed, a note will indicate the deletion.

Oversize materials (e.g., maps, drawings, charts) are reproduced by sectioning the original, beginning at the upper left-hand corner and continuing from left to right in equal sections with small overlaps. Each original is also photographed in one exposure and is included in reduced form at the back of the book.

Photographs included in the original manuscript have been reproduced xerographically in this copy. Higher quality 6" x 9" black and white photographic prints are available for any photographs or illustrations appearing in this copy for an additional charge. Contact UMI directly to order.

U·M·I

University Microfilms International
A Bell & Howell Information Company
300 North Zeeb Road, Ann Arbor, MI 48106-1346 USA
313: 761-4700 800: 521-0600

Order Number 1347057

**An experimental investigation of bevelled blade coating for
paper**

Altug, Mustafa Naci, M.S.

Western Michigan University, 1991

U·M·I
300 N. Zeeb Rd.
Ann Arbor, MI 48106

TABLE OF CONTENTS

ACKNOWLEDGEMENTS	ii
LIST OF TABLES	vi
LIST OF FIGURES	ix
NOMENCLATURE	xi
CHAPTER	
I. INTRODUCTION	1
II. REVIEW OF LITERATURE	8
The Coating Process of Paper	8
Blade Coating	9
Hydrodynamic Lubrication Theory	10
III. ANALYSIS OF THE MODELS TO BE TESTED	26
Lubrication Model	26
Impact Model	27
Combinations of Lubrication and Impulse Models	36
Lateral Force	36
IV. PROBLEM STATEMENT AND SIGNIFICANCE OF PROBLEM	38
V. OBJECTIVES	41
VI. EXPERIMENTAL DESIGN	42
Theoretical Approach	42
Experimental Approach	43
Operating Parameters	46

Table of Contents--Continued

	Mass Flow Rate	46
	Incoming layer Thickness	49
	Web Speed	50
	Blade Type and Dimensions	52
	Blade Bevel Angle	54
	Coating Color Formulation	57
	Absorption and Penetration Phenomena	57
	Viscosity of Coating Color	60
VIII.	EXPERIMENTAL RESULTS AND DISCUSSION	64
	First Pilot-Plant Trial	64
	Second Pilot-Plant Trial	65
	Third Pilot-Plant Trial	67
	Determination of Dynamic Forces	67
	At 600 fpm	67
	At 800 fpm	71
	At 1000 fpm	72
	Comparison of Results With the Models	72
	Prediction of Lubrication Theory	76
	Prediction of the Impact Model	80
	Combination of Impulse and Hydrodynamic Force	86
	Lateral Force Model.....	87
IX.	CONCLUSIONS	90

Table of Contents--Continued

APPENDICES 93

A. Derivation of the Hydrodynamic Force Based on Lubrication Theory 94

B. Determination of the Total Mass Flow Rate at Different Web Speeds 100

C. Derivation of The Corresponding Equation to Transfer the Tube Pressure at Tip of the Blade 117

D. Coating Color Formulation 121

E. Coat Weight Versus Web Speeds 124

F. Coat Weight Versus Blade Pressure Data for the Second Pilot-Plant Trial 132

G. Coat Weight Versus Blade Pressure Data for the Third Pilot-Plant Trial 147

H. Determination of the Incoming Layer Thickness 162

I. Calculation of the Hydrodynamic Forces Based on Lubrication Theory 164

J. Calculations of the Dynamic Forces based on Impact Model 166

REFERENCES 171

LIST OF TABLES

1. Effect of Operational Parameters on Coat Weight Volume, W	18
2. Relationship Between Coat Weight and Surface Roughness	35
3. Operational Parameters During Experimental Trials	47
4. Determination of Excess Coating Flow Rate (R1)	49
5. Mass Flow Rates at Different Web Speeds	49
6. Actual Versus Adjusted Web Speeds	52
7. Conversion Table to Determine Pressure at the Tip of the Blade	55
8. Basesheet Properties	60
9. Solid Content of Coating Color	61
10. Viscosity Values at Each Web Speed	63
11. Total Dynamic Forces at Each Web Speed	76
12. Determination of Upper and Lower Limits for the Effective Gap	79
13. Determination of Maximum Hydrodynamic Pressure Underneath the Blade Based on Lubrication Theory	79
14. Prediction of Dynamic Forces According to Impact Model at Each Web Speed	84
15. Comparison Between Experimentally Measured TDF and Calculated TDF According to Impact Model	85

List of Tables--Continued

16. Prediction of Impact Model as a Combination of Impulse and Hydrodynamic Force at Each Web Speed	86
17. Combination of Impulse and Hydrodynamic Lubrication Force at Each Web Speed	88
18. Corresponding Lateral Force at Each Web Speed	89
19. Mass Flow Rate of the Excess Coating Color	103
20. Data for the Determination of Basis Weight	105
21. Determination of Coat weight at 600 fpm and 30 psi	106
22. Determination of Coat weight at 800 fpm and 30 psi	109
23. Determination of Coat weight at 1000 fpm at 30 psi	111
24. Determination of R_2 at Each Web Speeds	115
25. Determination of Wet Coat Weight	115
26. Total Mass Flow Rate at Different Web Speeds	116
27. Formulation	122
28. Determination of Coat weight at 500 fpm and 25 psi	125
29. Determination of Coat weight at 750 fpm and 25 psi	127
30. Determination of Coat weight at 1000 fpm and 25 psi	129
31. Results	131

List of Tables--Continued

32. Coat Weight Versus Blade Pressure at 500 fpm	133
33. Coat Weight Versus Blade Tube Pressure at 500 fpm	137
34. Coat Weight Versus Blade Tube Pressure at 750 fpm	138
35. Coat Weight Versus Blade Tube Pressure 750 fpm	142
36. Coat Weight Versus Blade Pressure at 1000 fpm	143
37. Coat Weight Versus Blade Tube Pressure at 1000 fpm	146
38. Coat Weight Versus Blade Pressure at 600 fpm	148
39. Coat Weight Versus Blade Tube Pressure at 600 fpm	152
40. Coat Weight Versus Blade Pressure at 800 fpm	153
41. Coat Weight Versus Blade Tube Pressure at 800 fpm	156
42. Coat Weight Versus Blade Pressure at 1000 fpm	157
43. Coat Weight Versus Blade Tube Pressure at 1000 fpm	161

LIST OF FIGURES

1. A Common Type of Blade Coating With an Applicator Roll: So Called Flooded Nip Coater (4)	2
2. Two Different Systems Used for Blade Coating of Paper: (A) the Puddle Coater, (B) Blade Coater With an Applicator Roll (14)	3
3. The Two Modes of Blade Coating: (1) Bevelled Blade and (2) Bent Blade (14)	4
4. Effective Gap (h) Between Blade and Substrate (14)	15
5. Impulse Force, R_z , Acting on the Blade (2)	29
6. Pressure Force, P_z , Acting on the Blade (2)	29
7. Action of Blade Forces (2)	31
8. Hydrodynamic Force, H_z , Acting on the Blade (2)	31
9. Blade Pressure Transmission to the Paper (2)	33
10. Flow Chart of Trials	45
11. Collecting of Excess coating Color	48
12. Incoming Layer Thickness (h_1) and Wet Film Thickness (h_w) at Each Web Speed	51
13. Photomicrographs of the Blade Before and After use	56
14. Viscosity of Coating Color	62
15. Coat Weight Versus Web Speed	66

List of Figures--Continued

16. Coat Weight Versus Blade Pressure at 500 fpm	68
17. Coat Weight Versus Blade Pressure at 750 fpm	69
18. Coat Weight Versus Blade Pressure at 1000 fpm	70
19. Coat Weight Versus Blade Pressure at 600 fpm	73
20. Coat Weight Versus Blade Pressure at 800 fpm	74
21. Coat Weight Versus Blade Pressure at 1000 fpm	75
22. Hydrodynamic Lubrication Force as a Function of Effective Gap at 600 fpm	81
23. Hydrodynamic Lubrication Force as a Function of Effective Gap at 800 fpm	82
24. Hydrodynamic Lubrication Force as a Function of Effective Gap at 1000 fpm	83

NOMENCLATURE

- R_z = Impulse Force ($\text{kg}\cdot\text{m}/\text{s}^2$ or N)
- P_z = Pressure Force ($\text{kg}\cdot\text{m}/\text{s}^2$ or N)
- H_z = Hydrodynamic force (based on impact model) at the proximity of the blade ($\text{kg}\cdot\text{m}/\text{s}^2$ or N)
- F_{hy} = Hydrodynamic Force (based on lubrication theory) underneath the blade (kg/s^2 or N/m)
- T = Lateral Force (kg/s^2 or N/m)
- m = Mass flow rate (kg/s),
- V = Web speed (m/s),
- μ = Viscosity of the coating color underneath the blade ($\text{kg}/\text{m}\cdot\text{s}$),
- μ_1 = Viscosity of the coating color at the close proximity of the blade ($\text{kg}/\text{m}\cdot\text{s}$),
- d = Density of the coating color (kg/m^3),
- CW = Coat weight (kg/m^2),
- ϕ = Fraction of solid in coatings (%),
- α = Blade bevel angle,
- h_w = the thickness of the wet coating (m),
- h_o = Effective gap between blade and paper web (m),
- h_1 = Thickness of coating color reaching the blade (m),
- h_2 = Thickness of the incoming coating layer (m),
- t = Average thickness of roughness volume (m),

c = Thickness of the blade (m),
 s = Length of bevelled surface (m),
 W_1 = Width of the coated paper (m),
 X_1 = The distance from the application point of tube pressure to the tip of the blade (m),
 X_2 = The total length of the blade (m),
 X_3 = The distance from mounting of the blade to the application point of the tube pressure (m)
 F_2 = Tube pressure (kPa or Psi),
 F = Blade pressure at blade tip (kPa or Psi),
TDF = Total dynamic forces at blade tip (kPa or Psi)

CHAPTER I

INTRODUCTION

Blade coating is the most popular method of high speed coating in the paper industry. In this process, an excess amount of pigmented suspension is deposited on a moving web of paper by an applicator roll or extrusion device (Figures 1 and 2). Some distance downstream of the fluid supply, the excess amount is doctored off the substrate with a blade which is usually inclined at a predetermined angle to the backing roll.

Blade coating operations can be subdivided into two groups: bevelled blade coating (known as stiff blade) and bent blade (Figure 3). Bevelled blades are usually used for low coat weight grades, while bent blades are convenient for heavier coating grades (1). In this experimental investigation, only bevelled blades were used to coat the basesheet.

In bevelled-blade coating, coat weight is determined by the state of equilibrium of forces acting on the blade and paper. These are mechanical and dynamic forces. Many attempts have been made over the years to relate coat weight (or wet film thickness) to blade loading, angle, thickness, length, and mounting parameters of the blade

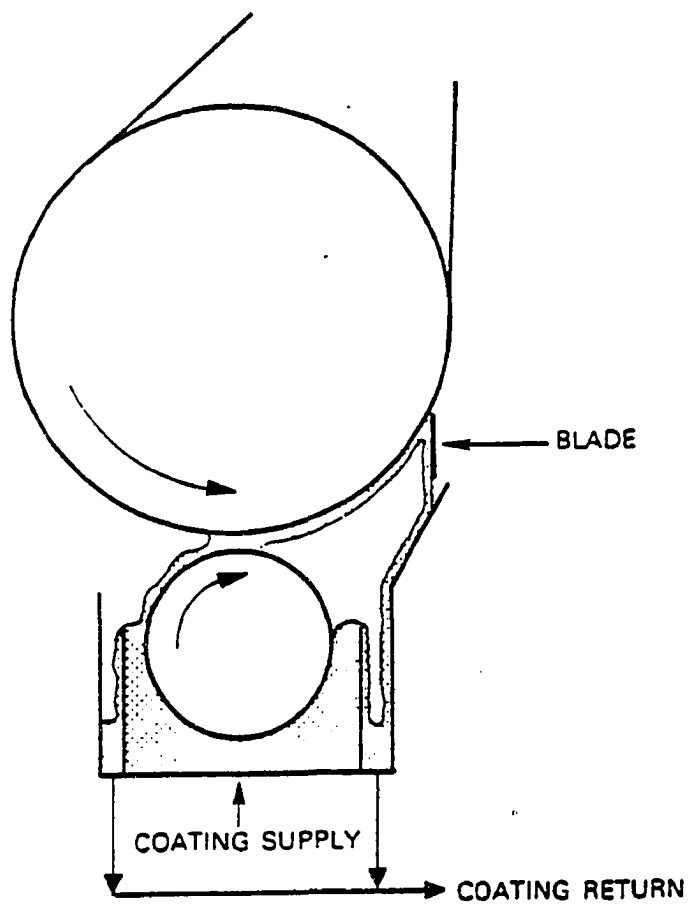
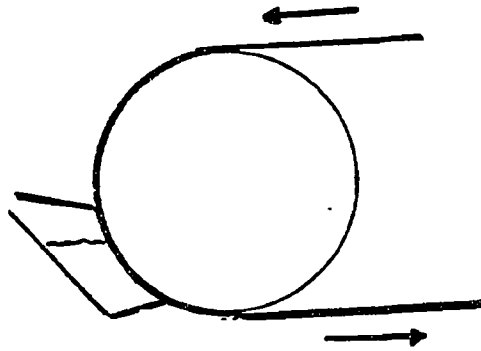
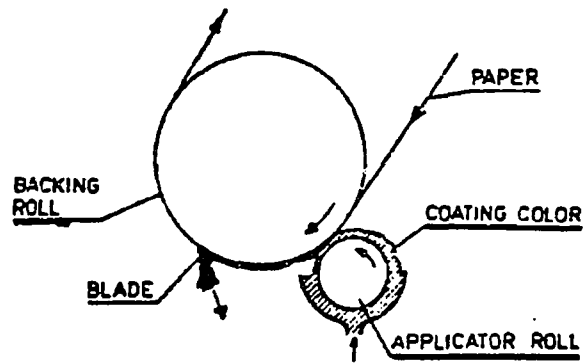


Figure 1. A Common Type of Blade Coating With an Applicator Roll: So-Called Flooded Nip Coater (4).

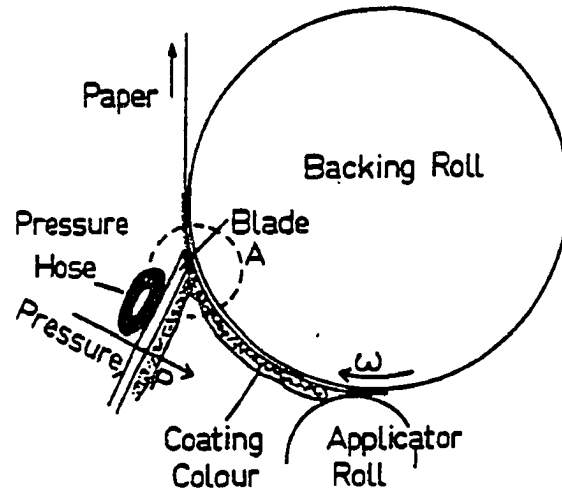


A

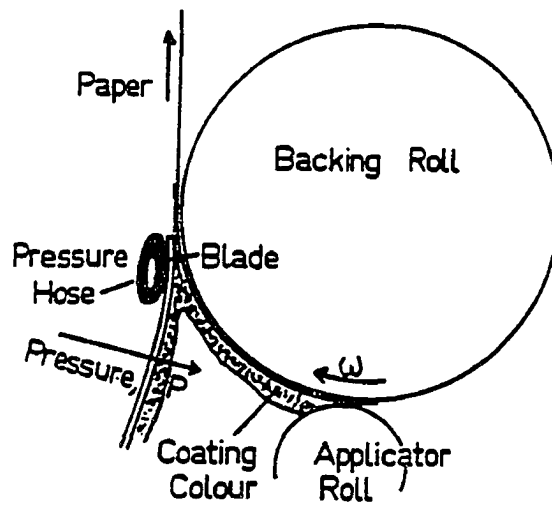


B

Figure 2. Two Different Systems Used for Blade Coating of Paper: (A) the Puddle Coater, (B) Blade Coater With an Applicator Roll (14).



TYPE 1: STIFF BLADE



TYPE 2: BENT BLADE

Figure 3. The Two Modes of Blade Coating: (1) Bevelled Blade and (2) Bent Blade (14).

and such other factors as web speed, and suspension viscosity (2-7). However, different researchers have reached divergent conclusions on the relative importance of the various factors affecting coat weight. As a result, different analytical and semi-empirical equations have been derived to define the total dynamic forces generated by the coating color during the coating process.

A widely accepted belief is that coating color in the nip region close to and under the blade develops a load bearing capacity, i.e., blade coating can be examined with the hydrodynamic lubrication theory (3-5). Theoretical predictions, based on this approximation, for the effects of independent variables on coat weight have generally been observed in practice (4). For bevelled blades, a decrease in coat weight can be achieved by: (a) increasing blade pressure, (b) decreasing the coating viscosity or solid concentration of coating color, (c) decreasing paper absorbency or roughness, (d) decreasing the blade thickness, (e) decreasing the web speed, and (f) increasing the bevel angle.

In contrast to the above approach, another belief suggests that the coat weight or the amount of coating color passing between the blade and the web is determined by the compressibility and the roughness of the paper. A popular analysis based on this hypothesis which predicts the relationship between blade pressure and coat weight has

been presented by Kahila and Eklund (2). These authors derived semi-empirical equations which correlate blade pressure and coat weight by considering the hydrodynamic lift at the close proximity of the blade tip but not underneath the blade. They proposed that in order to control coat weight, the applied external blade load should be adjusted according to the opposite forces generated by the incoming excess coating color. These forces are: impulse, pressure, and the hydrodynamic force.

In an attempt to better correlate operating and design parameters with coat weight in bevelled blade coating, Kuzmak (4) took into account the combination of these two popular analyses, namely lubrication theory and the impact model. He showed that to maintain a constant coat weight, there is a need for a steadily increasing blade load when running a bevelled blade on its heel and decreasing load when running the blade on its toe. Advancing this model a step further, Kartovaara (5) considered the lateral or shear force both underneath and in the close vicinity of the blade and he defined total dynamic forces as a summation of (a) impulse, (b) hydrodynamic, and (c) lateral forces. The lateral force has been neglected in the previous analyses.

The objective of this thesis was to test the existing models and to show which one could be best used to predict coat weight development under certain conditions of the

coating process. A typical offset basesheet was selected and treated to minimize its roughness, compressibility and absorptivity. Pilot-plant trials were performed by changing the web speed from 500 to 1000 fpm. Total dynamic forces acting on the bevelled blade were approximated based on experimental data at each web speed. Finally, the results from systematic pilot-plant trials were quantitatively compared with the predictions of: (a) lubrication theory, (b) impact model with pressure force, (c) impact model without pressure force, (d) the combination of impact and lubrication theory, and (e) lateral or shear force.

CHAPTER II

REVIEW OF LITERATURE

The Coating Process of Paper

In the coating process a fluid, namely air, is displaced on a moving porous solid surface by another fluid in order to deposit a uniform thin liquid film. The deposition of thin films on a moving web can be achieved with two primary approaches: (1) delivering the needed volume of liquid film and transferring it to the substrate, or (2) delivering excess liquid and metering it some distance downstream of the liquid supply.

Coating flows can be categorized as small scale, viscous, laminar, steady flows with free surfaces (6). In many coating processes the thin film is formed from a liquid puddle and flows through a narrow clearance between the application device and the moving substrate. This clearance varies in the flow direction so that the liquid pressure varies accordingly, much like in a lubrication journal bearing. The pressure in the vertical direction can deform the substrate and the applicator roll. This deformation varies the flow field, which in turn changes the hydrodynamic pressure that acts on the boundaries of the substrate and applicator (6).

In coating systems, the application unit distributes the fluid into a wide enough pond, and spreads the liquid locally so that the coated layer is uniform. Even slight cross-flow variations in the clearance between the applicator unit and the moving substrate produces nonuniformities both in local flow rate and in the coating layer. Precise machining of a rigid applicator device and nearly rigid backup roll is the way of achieving the requisite uniformity of flow (6).

The coating fluid is usually a pigmented suspension of mineral particles in water (i.e., clay, calcium carbonate, and titanium dioxide) ranging in concentrations of dry solids from 56 to 70% based on weight (7). The suspension also includes other chemicals such as binders, dispersants and additives.

Blade Coating

The blade coater is established as the most popular means of producing high quality coated printing paper at high speed. As it is known from practice, coat weight is related to the following: (a) coating color properties, (b) base sheet properties, and (c) operating conditions on the coater.

Until 1960, the existing experimental data indicate that coat weight is controlled by: (a) coating color solids and rheology, (b) base sheet surface properties, and

(c) blade pressure and machine speed (8).

Analysis of the basic mechanisms involved in blade coating began in 1960 with a paper published by Follette and Fowells (8). They considered the force acting on the blade generated by coating color. This force, which is opposite and equal to the external blade pressure, is referred as a hydrodynamic force which lifts the blade. These authors assumed that, during steady state operation, the blade tip forms a converging channel tangent to the backing roll. They proposed that the pressure exerted by a wedge of the fluid under the blade would be similar the one found in a rotating journal bearing. In the blade coater, the rotating paper on the backing roll forces a wedge of coating fluid under the blade and that causes a slight lifting of the blade. This force is balanced by the externally applied force, i.e., the blade load. After this first study, many publications followed based on the viewpoint that blade coating can be analyzed with hydrodynamic lubrication theory.

Hydrodynamic Lubrication Theory

The flow under the tip of the blade is similar to lubrication as in journal bearings with infinite length. As fluid enters the blade region, not all of it can go through. Some fluid will go underneath the blade, driven by the pressure buildup upstream, while another part of it

will be deflected away. As a result, the blade will be lifted up. This hydrodynamic lift is taken to be equal to the mechanical pressure applied externally on the blade.

The original development of lubrication theory was made by Osborne Reynolds (9). Basic assumptions involved in this theory are: (a) laminar flow conditions exist in the fluid film, (b) steady state conditions exist, (c) the liquid is Newtonian in flow behavior, (d) inertial forces are small with respect to shear forces, (e) fluid is incompressible and isothermal (i.e., constant density and temperature), (f) the pressure generated in the film is only a function of the horizontal direction, and (g) local fluid velocity is a function of both horizontal and vertical directions.

It is possible to calculate velocity, pressure and volumetric flow rate of the coating color under the blade. However, there are some inconsistencies between the lubrication approximation and what has been observed in practice. These are:

1. Lubrication does not consider free surfaces. It also neglects the impact force acting on the blade due to the motion of the coating color.

2. The web is not deformable, porous, or absorptive.

3. Uneven film thickness due to substrate roughness and penetration due to normal forces are not considered.

Two approaches have been considered to depict hydro-

dynamic effect of coating color under the blade. On one hand, a group of researchers, Follette and Fowells (8), Bliesner (25), Bohmer (10), Clark et al., (11) Modrak (12), Hayward (13), and Franckh and Scriven (6) supported the idea of converging channel between the blade and substrate. On the other hand, Turai (3), Gartaganis (14), Kuzmak (4), Hwang (15), Eklund and Kahila (2,16) approach the problem as if there is a parallel channel between blade and substrate. Follette and Fowells (8) published the following empirical equation to explain how coat weight is varied by changing blade pressure (P):

$$CW = B * P^A \quad [1]$$

where A and B are coefficients depending on suspension viscosity and solids content, web speed, blade angle, sheet roughness and absorbency. This equation works only for the bevelled type blade. Coat weight is directly proportional to the wet film thickness according to the equation below:

$$h_w = \frac{CW}{(\phi * d)} \quad [2]$$

where h_w = wet film thickness (m)

CW = coat weight (kg/m²)

ϕ = the fraction of solid in coatings (%),

d = the density of the suspension (kg/m^3).

An analysis of the geometry at the tip of a blade and the system as a lubrication problem was presented by Bohmer (10). He also studied the effects of different variables on the wet coating thickness and concluded that this is influenced by the following three phenomena:

1. Filling in the cavities of the base paper, which is dependent on the base paper roughness, its compressibility and blade pressure: This is true not only because the paper is compressed but also because higher pressure forces the pigment suspension deeper into the cavities of the paper.

2. Penetration of water and binder into the paper: This process depends on the degree of sizing and pore structure of the paper, the water retention of the coating color, pressure normal to the substrate and the time available for this penetration. The first two variables may be expressed in more fundamental terms, such as the dynamic contact angle and surface tension. The third is a direct function of machine speed and the distance from the application point to the blade.

3. The action of the blade which is influenced by both the machine speed and rheological properties of the coating color: These properties are a function of solids content, and therefore influenced by penetration. The action of the blade will also be affected by blade

parameters, such as blade width, angle and pressure.

Turai (3) analyzed the bevelled blade coater and published the derivation of a mathematical model by considering the flow underneath the blade (Figure 4) as a two-dimensional laminar flow between two parallel straight

$$v = \left(\frac{V}{h_o}\right)y - \left(\frac{dP}{dx} * \frac{h_o y - y^2}{2\mu}\right) \quad [3]$$

walls. In Equation 3, the first term represents the velocity component due to the drag effect of the stationary blade, called drag flow. The second term represents the velocity component due to the pressure gradient acting in the horizontal direction (i.e., direction along the movement of the web) and it is called pressure flow. According to Turai (3), the mechanical pressure which is applied externally on the blade is balanced by the fluid pressure due to compressibility of the paper. This causes an indentation of the paper surface as the paper passes through the nip. This situation, combined with wearing of the blade, forms a parallel channel between the blade and substrate. Therein the pressure gradient is zero at the nip. In other words, the pressure in both ends of the channel is assumed ambient and the flow is characterized as a simple-shear Couette flow. Turai also proposed a stagnation plane at the location where drag forces are

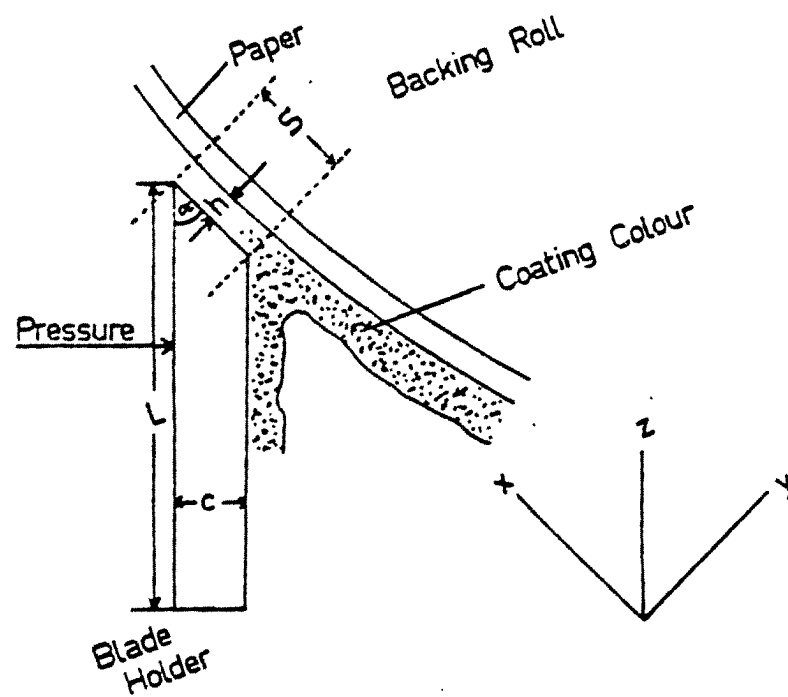


Figure 4. Effective Gap (h) Between Blade and Substrate (14).

Reproduced with permission of the copyright owner. Further reproduction prohibited without permission.

balanced by pressure forces. This plane leads to solid particles settling out of the suspension. Such a phenomenon causes blade scratches. Finally, to avoid formation of a stagnation plane, the pressure flow should be less than one third of drag flow.

Ginn (17) considered the flow not only under the tip but also in the converging channel along the blade length. He identified the development of a stagnation plane very close to the entrance of the blade nip, something that was first reported by Modrak (12). This plane separates the region of downstream flow from backflow. According to Ginn (17), the blade tip can be simulated by a generalized Couette flow in a parallel channel where blade wear is presumed from the shear stresses at the blade surface. Thus the film thickness through the nip is a function of relative driving forces of web movement and fluid stresses.

Guzy and Higgins (18) considered a hydrodynamic pressure drop across the nip to account for the developing free surface at the trailing end of the blade and to differentiate between possible flows upstream. Their theoretical analysis indicated that when the pressure drop (i.e., exit minus inlet) is positive, there is an upper limit on the final film thickness and, thus coat weight. When it is negative, there is no limit on coat weight. An interesting observation from this analysis is that if the

pressure in the pond becomes subatmospheric, there is an upper limit on wet film thickness and the process becomes unstable as the final film thickness decreases.

Gartaganis (14) did a series of experiments and published empirical equations which correlated operational parameters with total coating thickness by using Turai's mathematical model for blade coating process. This work is summarized in Table 1.

All of the above analyses speculated that the hydrodynamic phenomenon, more or less influenced by absorption, constitutes the principal mechanism of coating deposition. In these models, the hydrodynamic lift is taken equal to blade loading and the blade considered as a cantilever beam.

In contrast to the hydrodynamic lubrication theory, Windle and Beazley (19), and Kahila and Eklund (2,16) support a separate idea which is different than the one presented above. Their hypothesis is that coat weight is controlled by the compressibility and roughness of base paper rather than the hydrodynamic lift. These authors accounted for sheet roughness and compressibility of paper. Windle and Beazley tried to show the effect of normal forces contributing to the hydrodynamic lift. However, they were not successful in showing experimentally that normal forces influence coat weight, but they were (20) the first to discuss viscoelasticity of coating

Table 1

Effect of Operational Parameters on Coat Weight Volume, W

INCREASE IN VARIABLE	BEVELLED BLADE
WIDTH OF BLADE (b)	INCREASES WITH b
COATING VISCOSITY (μ)	INCREASES WITH $\mu^{0.5}$
MACHINE SPEED (V)	INCREASES WITH $U^{1.5}$
BLADE PRESSURE (P)	DECREASES WITH $p^{0.5}$
BLADE THICKNESS (c)	INCREASES WITH $c^{0.5}$
BLADE BEVEL (α)	DECREASES WITH $\sin\alpha^{0.5}$
BACKING ROLL RADIUS (m)	NOT APPLICABLE
BLADE EXTENSION (L)	NOT APPLICABLE

$$CW = (\text{SPEED})^{1.5}$$

$$CW = (\text{VISCOSITY})^{0.5}$$

$$CW = (\text{BLADE THICKNESS})^{0.5}$$

color.

Eklund and Kahila (2,16) calculated the dynamic forces acting on the blade as the coating layer, transferred by the applicator roll on to the base stock, strikes the underside of the blade and changes direction. They defined three dynamic forces: an impulse force, a pressure force, and a hydrodynamic force. Coat weight is determined by the interactions between the compressive force which is exerted on the blade and by the surface

properties of the paper. The space between the blade and the paper which is filled by coating color is variable depending on the compressive load and wet compressibility of paper. The compressive force exerted by the blade on the paper is a resultant of the differences between the mechanical blade load, F_z , and the total dynamic forces generated by the coating color (Equation 4). This compressive force (or net resultant force), F_o , acting on the web is determined by using Equation 5 (2).

$$TDF = [R_z + P_z + H_z] \quad [4]$$

$$F_o = [F_z - (TDF)] * \text{Cos}\alpha \quad [5]$$

where F_z = blade load (kPa),

R_z = impulse force (kPa),

P_z = pressure forces (kPa),

H_z = hydrodynamic forces (kPa).

In an attempt to better correlate operating and design parameters with coat weight in bevelled blade coating, Kuzmak (4) took into account the hydrodynamic pressure term developed by Turai (3) for bevelled blade coating (Equation 3). In addition, he also considered the impulse approximation of Kahila and Eklund (2). The derived equation for total wet coating thickness as a function of these forces is shown in Equation 6.

$$h_t = h_m + K_1 \left[\frac{6K_2 \mu s^2 V \cos \alpha}{(kP_G - a_1 F_m)} \right] \quad [6]$$

where h_t = the total wet coating thickness (m),

h_m = the minimum coating film thickness (m),

μ = viscosity of the coating color (kg/m-s),

s = the length of bevel surface (m),

V = web speed (m/s),

α = the bevel angle,

P_G = the blade gauge pressure (N/m²),

F_m = the force exerted by the coating striking the side of the blade (N),

a_1 = a coefficient giving the component of F_m ,

K_1, K_2 = a constant which converts the gauge pressure to the mechanical force per unit width of the blade.

This model was verified experimentally in a pilot plant where the effects of bevel surface area, fluid viscosity, blade heel, and toe on coat weight were studied. Key conclusions were:

1. When the bevel surface is parallel to the paper surface, a constant coat weight is maintained. When the blade runs on the bevel heel, however, the blade pressure must be continuously increased to maintain constant coat weight. Conversely, when the blade runs on its toe, the

blade pressure should be decreased continuously. The heel and toe effect is one of the reasons which explains unsteady state situations existing during coating operation. Other reasons for coat weight variations might be: (a) change in coating color viscosity, (b) change in base stock roughness and absorptivity, and (c) existence of substantial normal forces.

2. Wet coating thickness is dramatically changed when the bevel surface area is changed, while all other variables are kept constant. The higher the surface area of the blade, the thicker the wet film thickness.

3. As viscosity decreases, the change in coating thickness with blade pressure approaches zero. That is, at some low viscosity, changing the blade pressure produces no change in the wet film thickness.

The lateral force, or the shear, underneath the blade has been neglected in the previous analyses. Kartovaara (5) has done experiments to determine the lateral force at the close vicinity and underneath the bevel blade. He derived Equation 7 to calculate this force (T):

$$T = \left[\frac{V \cdot s \cdot \mu}{2 \cdot (h_w - t)} \right] + [V \cdot \mu_1] \quad [7]$$

where T = lateral force per unit length (N/m),

V = web speed (m/s)

s = bevel width (um),

μ = viscosity underneath of the blade (kg/m-s),

μ_1 = entrance viscosity (kg/m-s),

h_w = thickness of the wet coating (um),

The first term represents the shear force underneath the blade and the second term represents the shear force developed at close proximity to the blade tip. According to his study, the lateral force should not be neglected, because it is about 30% of the TDF.

Pranckh and Scriven (6) developed a physical model for blade coating based on the elastohydrodynamic theory. They calculated the effects of operational parameters, such as blade loading and stiffness, substrate velocity, incoming layer thickness, viscosity and surface tension, blade bevel angle and elasticity of substrate on coat weight. The basic equations were solved by considering all of the forces acting together to show the effect of these parameters on coat weight. A computer model estimates the steady state data for the velocity and pressure fields, stream lines, and velocity and shear rate contours for both Newtonian and non-Newtonian fluids. The major advantages of this model are: (a) it encompass the simple slit flow model of Turai (3), (b) the impulse approximation put forward by Kahila and Eklund (2) and discussed by Kuzmak (4), and (c) the lubrication approximation worked out by Chen and Scriven (22) and the rigid blade model for shear thinning liquids as discussed by Sullivan et al.

(21). The model advances modeling of blade coating in three respects:

1. It enlarges the elastohydrodynamic analysis by Chen and Scriven (22) to take into account inertial effects and it replaces the one-dimensional flow approximation with a two-dimensional flow of shear thinning fluid.

2. It takes into account the compressibility of the substrate and backup roll. This can be important, because the shape of the metering gap and the distribution of the liquid pressure in that gap depends on the deformability of the substrate and its backup.

3. It includes free surface effects immediately before the blade, where excess coating liquid is turned away and just after the blade where velocity within the coating relaxes into simple translation with the substrate.

Pranckh and Scriven (6) investigated the previous theories by testing them mathematically with results from their computer model. Their conclusions were: (a) the blade may not be a simple cantilever beam, (b) the blade may not be parallel to the substrate surface, and that may not remain planar--the gap may instead be converging or diverging; (c) the pressure gradient may be far from uniform under the blade, (d) Eklund and Kahila (2) used the momentum change of the excess coating as a pressure

force and impulse force in their model--this momentum change of the excess color should be counted either as momentum flux or as the equivalent pressure forces; and (e) the lubrication approximation excludes the inertial effects in high speed blade coating. It also takes the flow as nearly one dimensional, so the free surface effects upstream and downstream of the gap are neglected.

The penetration of liquid into the porous substrate was analyzed by Chen and Scriven (22). They considered the penetration of liquid on to the paper. They proposed that while the penetration rate is mostly affected by the external hydrodynamic force at both application and metering zones, capillary force controls the penetration in the transit zone. They concluded that the influence of the dwell time is considerably less than that of the hydrodynamic force. They calculated that the hydrodynamic pressure at the blade metering zone is about six times greater than the one in the applicator zone.

Predictions based on the above models for the effects of independent variables on wet film thickness (or coat weight) have generally been successful in practice. All of these analyses, except Kahila and Eklund's (2) impulse approach, are based on lubrication theory. In these models, the hydrodynamic lift is taken equal to the blade loading. The basic assumption in lubrication theory is that a two-dimensional flow field can be represented by a

one-dimensional model, i.e., the pressure is only a function of downstream coordinates. An important characteristic, however, which has been ignored in the previous studies, except the one by Pranckh and Scriven, is that blade coating flows always include free surfaces. For incompressible fluids of constant viscosity, the fluid flow is governed by momentum conservation equations, which are made non-linear by the inertia term. In blade coating operations inertia effects in the nip are small enough to be neglected but the term due to free surfaces introduces an additional non-linearity which can not be avoided (6). In addition, none of the above analyses has considered the effect of liquid penetration in combination with the forces on coat weight simultaneously as a whole mechanism. Therefore, it would be interesting to test these models with their equations and to show whether or not any of these approaches could be used to determine the coat weight pickup under certain controlled conditions.

CHAPTER III

ANALYSIS OF MODELS TO BE TESTED

Lubrication Model

In this study, Turai's (3) equation (Equation 8) was tested to show whether or not total dynamic forces could be represented with only hydrodynamic lubrication theory. If not, the question was what percent of the total dynamic forces could be explained by lubrication theory.

$$F_{hy} = \frac{6\mu s^2 V}{h_o^2} \left(1 - \frac{2h_w}{h_o}\right) \quad [8]$$

where F_{hy} = hydrodynamic force per unit length underneath the blade (N/m),

s = the length of bevelled surface (μm),

h_o = the coating thickness experiencing shear (μm),

h_w = the thickness of the wet coating (μm),

μ = coating color viscosity (kg/m-s),

V = web speed (m/s).

The derivation of Equation 8 is presented in Appendix A.

Many researchers believed that the total dynamic forces could not be explained exclusively by the hydrodynamic lubrication theory. However, most of them supported

the idea that hydrodynamic lift underneath the blade was the dominating force controlling coat weight development. The problem is that nobody has presented experimental data to demonstrate this idea clearly. For that reason, one of the main objectives of this study was to obtain experimental data which could contribute to understanding of this question.

Impact Model

According to this analysis, coat weight is determined by the compressibility and the roughness of the paper. Eklund and Kahila (2,16) defined total dynamic forces as a summation of impulse, pressure, and hydrodynamic force. The description of each dynamic force based on Eklund and Kahila's model (2) is presented below.

1. The impulse force (R_z) is generated when excess coating color strikes the underside the blade and changes direction. The change of momentum induces an impulse type (Figure 5) force. It was derived by assuming: (a) frictional losses can be neglected, and (b) the velocity of the coating color is constant. It is calculated by using Equation 9.

$$R_z = m * V * \frac{(1 + \cos\alpha)}{\sin\alpha} \quad [9]$$

where m = the mass flow rate (kg/s),

V = the velocity of the coating color or web speed
(m/s),

α = the blade bevel angle.

2. The pressure force (P_z) is generated by the accumulation of coating color in the wedge-shaped domain formed between the blade and paper (Figure 6). This may cause local alterations in color velocity. A speed induced pressure force will arise. This force was derived based on non-frictional and laminar flow. It is calculated by using the equation shown below:

$$P_z = \frac{1}{2} mV \frac{\pi}{\alpha} * \left[1 - \left(0.5 - \frac{1}{\pi} \right) \frac{h_o}{h_2} \right] * \left[1 - \frac{1}{2 \frac{\pi}{\alpha} - 1} \right] * \left[\frac{1}{1 - \left(0.5 - \frac{1}{\pi} \right) \frac{h_o}{h_2}} \right]^2$$

where h_o = the thickness of coating color passing under the blade tip (μm),

h_2 = the thickness of coating color reaching the blade (μm).

3. The hydrodynamic force (H_z) is generated by the lubrication flow under the blade tip. Kahila and Eklund (2,16) propose when the tip of the blade is parallel to the paper surface, no hydrodynamic force will develop underneath the blade. The assumption is that the blade tip angle, α , (Figure 7) between the blade and substrate is equal to zero. However, a hydrodynamic force develops

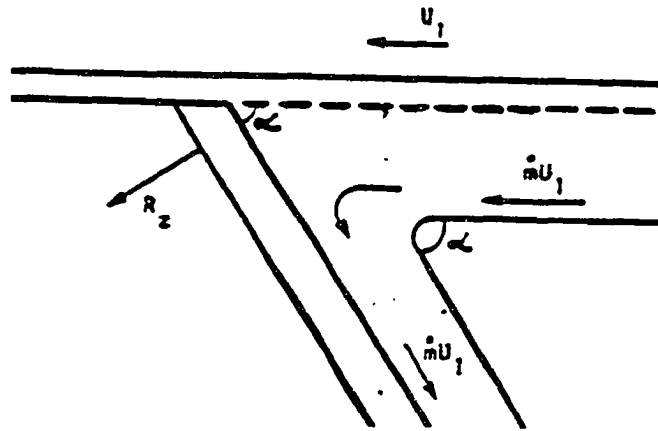


Figure 5. Impulse Force, R_z , Acting on the Blade (2).

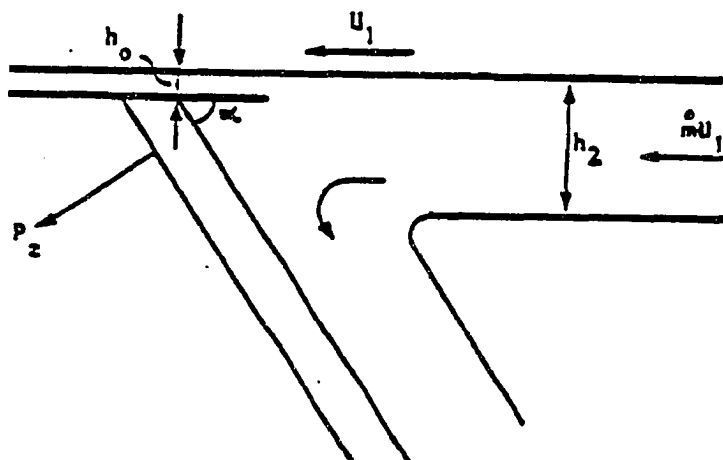


Figure 6. Pressure Force, P_z , Acting on the Blade (2).

in the close proximity to the blade edge (i.e., before the heel of the blade tip), where the coating color no longer flows down along the blade (Figure 8). This force can be calculated by using Equation 11.

$$HZ = \frac{6\mu_1 V}{\tan^2 \alpha} * [\ln 1+r - \frac{2*r}{2+r}] \quad [11]$$

where h_1 = the thickness of coating color reaching the blade (um),

$$r = h_1/h_0 - 1.$$

These authors showed that the hydrodynamic force at the proximity to the blade (or side-blade) can be neglected when the blade angle is above 27 degrees (2).

The mechanical force (F_z) acting on the blade loads the blade so that the edge of the blade presses the paper against the backing roll. Since all of the dynamic forces act in the direction which detach the blade from the paper surface, the opposing blade force should be at least equal to or greater than the TDF in order to have a stable situation during the coating process.

In the blade coating process, there is some distance between the application point of the tube pressure (X_1) and the tip of the blade (Figure 9). The corresponding blade pressure applied at the tip of the blade can be calculated by converting the tube pressure. Equation 12

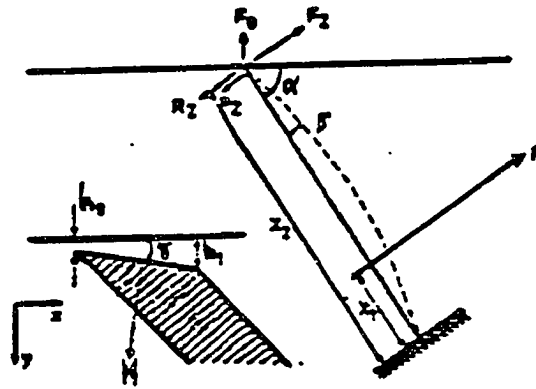


Figure 7. Action of Blade Forces (2).

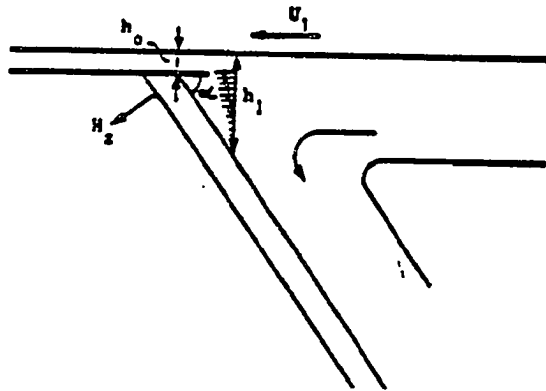


Figure 8. Hydrodynamic Force, H_z , Acting on the Blade (2).

is used for the conversion of the tube pressure at the tip of the blade.

$$F = \left[1 + \frac{1}{2} * \left(\frac{X_1}{X_2} \right)^3 - \frac{3}{2} * \frac{X_1}{X_2} \right] * F_z + \frac{3 D W}{X_2^3} \quad [12]$$

where X_1 and X_2 = blade dimensions,

W = deflection of the blade tip,

D = stiffness index of the blade,

E = Youngs's modulus of elasticity.

This equation is used to transfer the tube pressure from the application point (X_1) to the tip of the blade in order to calculate the exact blade force acting on the blade (2).

The compressive force (F_o) which is exerted by the blade on the paper is a result of the mechanical blade force and TDF. It is calculated by taking the difference of the mechanical load (F_z) and TDF as shown in Equation 13.

$$F_o = [F_z - (TDF)] * \cos\alpha \quad [13]$$

The main idea in this approach is that the coat weight is determined by the combined influences exerted by the paper compressing force (F_o) and surface properties of the paper. In the blade coating process, the blade presses

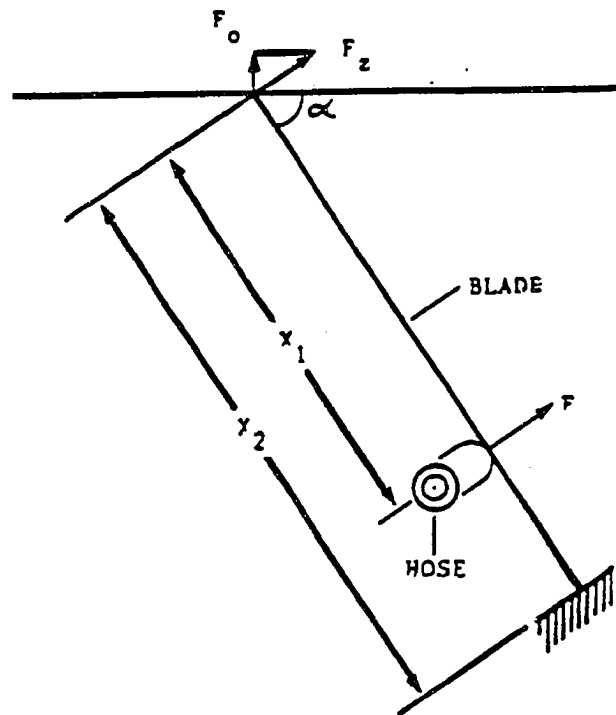


Figure 9. Blade Pressure Transmission to the Paper (2).

against the topmost fibers of the paper and the coating color is able to fill the free space that remains underneath the blade. Thus, the roughness of the paper is one of the most significant factors that affects the amount of coating color passing under the blade. As paper is compressible, the roughness volume of its surface will also change when the F_o is changed. When the blade force exceeds the total dynamic forces (i.e., $F_z > TDF$) there will be a net resultant force, F_o , exerted by the blade on the paper. The higher the F_o , the more the paper is compressed and the surface volume decreases so that coat weight reduces. When the force F_o decreases, i.e., by decreasing the F_z or increasing the TDF, the paper will expand. Upon expansion, the surface roughness volume increases and, accordingly, coat weight increases. When the net resultant force, F_o , approaches zero, i.e., the difference between F_z and TDF approaches zero, the paper achieves its most expanded state. In this situation the surface roughness volume of the paper becomes maximum and the coat weight reaches its maximum value. Table 2 shows how coat weight is affected by either changing F_z or TDF based on the impact model (2).

In this study, while the impact model was evaluated, each dynamic force (i.e., impulse, pressure, and hydrodynamic force) was calculated separately to show which one of these three forces was the dominant force during the

Table 2

Relationship Between Coat Weight and Surface Roughness (2)

F_z	TDF	F_o	Surface roughness	Coat wt.
INCR.	CONS.	INCR.	DECREASE	DECREASE
CONS.	INCR.	DECR.	INCREASE	INCREASE
$F_z =$	TDF	ZERO	MAXIMUM	MAXIMUM

coating process. In addition, whether or not coat weight development could be predicted without considering the hydrodynamic force both underneath and at close proximity of the blade was also investigated. Kahila and Eklund and (2) suggested that side-blade hydrodynamic force could be neglected when the blade angle was greater than 27 degrees. In pilot-plant trials conducted for the present study the blade angle was set at 45 degrees. Finally, this model was also tested by neglecting the pressure force, i.e., TDF were defined as a summation of only impulse force and hydrodynamic force at the vicinity of the blade tip. The reason for this was to check whether or not the momentum change of the excess coating color had been counted twice in the impact model by considering both impulse and pressure force as proposed by Pranchh and Scriven (6).

Combination of Lubrication and Impact Models

In an attempt to better correlate operating and design parameters with coat weight in bevelled blade coating, Kuzmak (4) took into account both the hydrodynamic force underneath the blade (Equation 8) developed by Turai (3) and the impulse force (Equation 9) from the impact model. Based on his experimental study, he concluded that the hydrodynamic force underneath the blade could not be neglected because this force was dominant dynamic force.

In this study, Kuzmak's approach was investigated by equating TDF to the summation of hydrodynamic and impulse force (Equation 14). For each web speed, the TDF measured from the pilot-plant trials was compared with the prediction Equation 14. Finally, the hydrodynamic and impulse forces were calculated separately and compared quantitatively with each other to find which one of the two controls coat weight. (In Equation 14, symbols are the same as in Equation 8 and 9).

$$TDF = \left[\frac{6\mu s^2 V}{h_o^2} \left(1 - \frac{2h_w}{h_o}\right) + \frac{1}{2} mV \frac{(1 + \cos\alpha)}{\sin\alpha} \right] \quad [14]$$

Lateral Force

Advancing Kuzmak's (4) approach a step further,

Kartovaara (5) considered the lateral or shear force in his experimental study. He defined TDF as a summation of hydrodynamic force underneath the blade, impulse, and lateral force as shown in Equation 15. (In Equation 15, symbols are the same as in Equation 7, 8, and 9).

$$TDF = \left[\frac{6\mu S^2 V}{h_o^2} \left(1 - \frac{2h_w}{h_o}\right) \right] + \left[\frac{1}{2} mV \frac{(1 + \cos\alpha)}{\sin\alpha} \right] + \left[\frac{VS\mu}{2h_w - t} + V\mu_1 \right] \quad [15]$$

Lateral forces both underneath and at close proximity to the blade were neglected in the previous analyses. Kartovaara (5) derived Equation 7 to calculate the lateral force in both regions. From experiments, he concluded that lateral force should not be neglected in a force equilibrium balance, because it was about 30% of the TDF. Therefore, another goal of this study was to investigate whether or not this force could be neglected.

CHAPTER IV

PROBLEM STATEMENT AND SIGNIFICANCE OF PROBLEM

Many attempts have been made to explain the dynamic forces acting on the blade. Different mathematical analyses of the bevelled blade coating process were derived to calculate the TDF. The previous analyses of paper coating that considered forces acting on a stiff bevelled blade included the lubrication, impact, combination of lubrication and impact, and lateral force models. However, none of the equations derived based on these models was tested with experimental data, except Kuzmak's study (4).

In this study, the pilot-plant trials were designed to determine the TDF at three different web speeds. Predictions of each model was calculated under the conditions occurring the experimental trials. Therefore, $(TDF)_{exp.}$ and $(TDF)_{calc.}$ were compared quantitatively for each model.

Based on lubrication theory, the TDF was explained with only the hydrodynamic lift underneath the blade. The main question is whether or not the TDF can be explained with only the hydrodynamic lift. If not, what percent of TDF belongs to hydrodynamic force underneath the blade.

In contrast to lubrication model, the impact model proposed that hydrodynamic force can not develop under-

neath the blade when the gap in between paper and blade is assumed parallel. Therefore, Kahila and Eklund (2) suggested that the hydrodynamic force should be considered at close proximity to the blade rather than underneath the blade. They defined the TDF as a summation of impulse, pressure and hydrodynamic forces. According to this analysis, while the impulse force is the dominant force, coat weight development can be predicted without considering the hydrodynamic forces when the blade angle is larger than 27 degrees. Therefore, the main questions for impact model are: (a) Does it predict the coat weight development? If it does, which one of these forces is the dominant force controlling coat weight? (b) Is it possible to predict coat weight development without considering the hydrodynamic force?

Pranckh and Scriven (6) suggested that the momentum change of excess coating color should be counted either as momentum flux or as the equivalent pressure forces in impact model (6). Therefore, they concluded that in the impact model, the momentum change of the excess coating color was counted twice by considering both the impulse and pressure forces. After that observation, Eklund (16) defined TDF as the summation of only impulse and hydrodynamic forces. However, there was no experimental verification of these claims. Therefore, this project experimentally investigates whether the impact model should be

considered as a summation of three dynamic forces or as a summation of only the impulse and hydrodynamic forces.

Finally, the lateral force will be calculated to investigate the extent to which coat weight development depends on this force. This is important because all of the previous models, except the one proposed by Kartovaara (5), assume that the lateral force is negligible and does not enter into the force balance.

CHAPTER V

OBJECTIVES

The objectives of this study are:

1. To determine the correlation between experimental data from controlled pilot-plant trials and calculated data obtained from the existing models, i.e., lubrication, impulse, lateral force, and combinations of these.

2. To determine whether coat weight development can be predicted by considering only impulse and pressure force.

3. To determine the magnitude of dynamic forces and to show which one of these dynamic forces plays the dominant role in controlling coat weight.

4. To determine whether or not lateral forces can be neglected in the force equilibrium balance around the blade.

5. To investigate whether or not the momentum change of excess coating color has been counted twice in the impact model.

CHAPTER VI

EXPERIMENTAL DESIGN

Theoretical Approach

In the coating process, the compressing load or the net resultant force which is exerted by the blade onto the paper is a resultant of the mechanical load (blade pressure) and the dynamic forces generated by the coating color. Dynamic forces, $(TDF)_{exp.}$, acting on the blade become constant, as soon as the coating process reaches the steady state. Coat weight development is controlled by adjusting the blade pressure. When the blade tube pressure, F_z , is reduced, the difference between F_z , and $(TDF)_{exp.}$ decreases as shown in Equation 16. As a result, the paper is able to expand to some degree and coat weight

$$F_o = [F_z - (TDF)_{exp.}] * \cos\alpha \quad [16]$$

increases until the system reaches a new state of equilibrium. The difference between F_z and $(TDF)_{exp.}$ will be smaller by further reduction of F_z . The smaller the difference between these two opposite forces at the blade tip, the higher will be the coat weight and the more sensitive will be the system reaction to small force

changes. If the TDF exceeds the F_z , then the blade will detach from the paper and coat weight will increase rapidly. This rapid increase of coat weight with an incremental decrease of F_z is the key to determining the critical blade load, $(Fz)_{critical}$, which is equal to $(TDF)_{exp.}$. The determination of $(Fz)_{critical}$ was the focus of this project.

Experimental Approach

In this thesis work, the existing models that have been proposed to determine TDF for the bevelled blade coater were evaluated with experimental data. The proposed models tested were: (a) the hydrodynamic lubrication theory, as analyzed by Turai (3), (b) the impact model derived by Kahila and Eklund (2), (c) combinations of lubrication and impact model, as proposed by Kuzmak (4), and (d) the lateral force, as derived by Kartovaara (5). The goal was to determine whether these models predict coat weight development on the paper web.

The methodology to realize the objectives of this thesis study comprised of pilot-plant trials. The Western Michigan University, Kalamazoo, pilot-plant coater was used for this project. The goal of the pilot-plant trials was to measure the dynamic forces, $(TDF)_{exp.}$, at speeds of 600, 800, and 1000 fpm. Three different trials were conducted by using the same type of paper. A logic

diagram depicting the sequential steps is presented in Figure 10. The first trial was done to determine to what extent coat weight was affected by absorption and penetration within the range of selected web speeds. This trial was necessary because all of the existing equations were derived as if the paper was nonabsorbent, i.e., the penetration of continuous phase in the paper web was neglected. Therefore, in order to test the existing models, operating conditions need to ensure that coat weight was not affected greatly by absorption and penetration phenomena. For that reason, in the first trial coat weight data were obtained by increasing the web speed from 500 to 1000 fpm in order to identify that dynamic forces were dominant.

The second trial was conducted to determine the blade pressure range which was about equal to $(TDF)_{exp.}$ at each web speed. Because the actual value of the $(TDF)_{exp.}$ under the experimental conditions was unknown, coat weight data were obtained first at high blade pressures (about 45 psi) and then pressure was reduced progressively to 5 psi. Therefore, three different sets of coat weight data were collected as a function of blade pressure. The first set of data was obtained by running the coater at 500 fpm web speed. Then, the second and third sets of data were obtained at 750 and 1000 fpm respectively (Figure 10). Later, the corresponding coat weight versus blade pressure

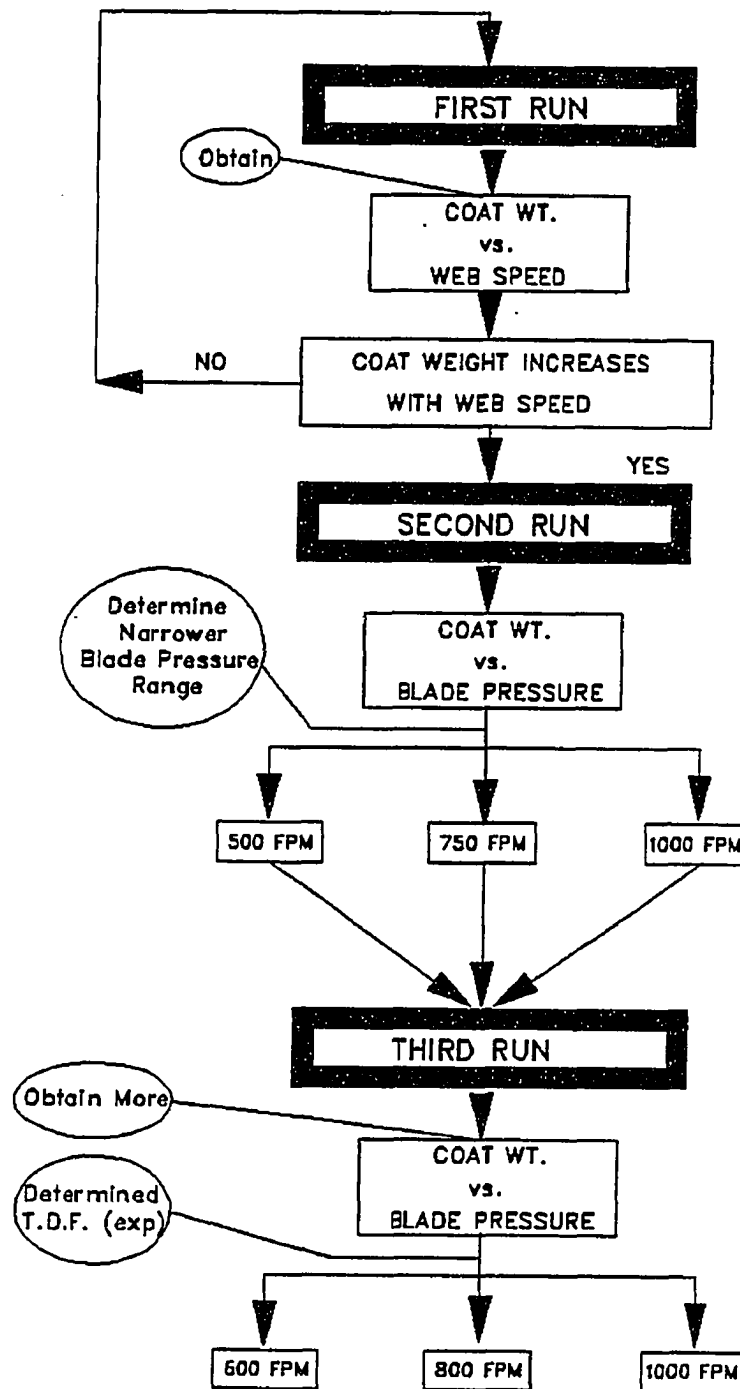


Figure 10. Pilot-plant trials.

graphs were drawn separately for each web speed so that narrower blade pressure ranges were determined for the third trials. The third trial was repeated within the predetermined blade pressure ranges, but web speeds were 600, 800, and 1000 fpm. Thus, more coat weight data were obtained while the blade pressure was decreased by one psi decrements and $(TDF)_{exp.}$ were determined at each web speed.

Operating Parameters

Three different experimental trials were done to determine $(TDF)_{exp.}$ at 600, 800, and 1000 fpm. Each set of coat weight data was obtained by changing the blade tube pressure at constant web speed. The mechanical and fluid parameters considered during each pilot-plant trial listed in Table 3.

Mass Flow Rate

In all trials, an attempt was made to maintain the mass flow rate of coating color supplied by an applicator roll constant. For each web speed, total mass flow rate was determined in two steps. First, the flow rate of the excess coating color (R_1) striking the blade was experimentally determined. This was achieved by collecting the excess coating after striking the blade, i.e., the recycle of excess coating color to the pond was not allowed. The

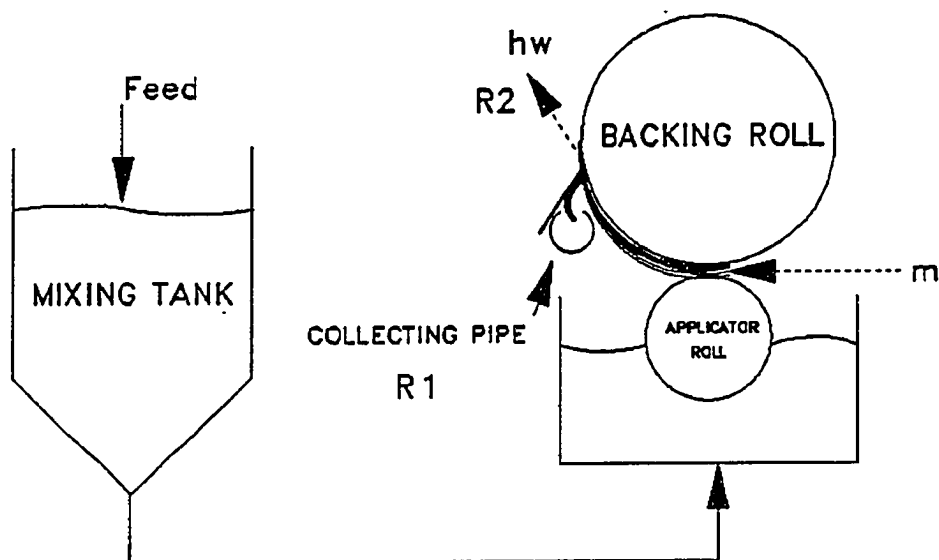
Table 3
Operational Parameters During the Experimental Trials

	UNITS	RUN 1	RUN 2	RUN 3
BLADE PRESSURE :	kPa	C	V	V
BLADE ANGLE :	Degree	C	C	C
BLADE THICKNESS :	um	C	C	C
BLADE DIMENSIONS :	mm	C	C	C
MASS FLOW :	Kg/s	C	C	C
WEB SPEED :	m/s	V	C	C
COLOR SOLIDS :	%	C	C	C
COLOR DENSITY :	Kg/m ³	C	C	C
COLOR VISCOSITY :	Kg/m-s	C	C	C
COAT WEIGHT :	g/m ²	V	V	V

C : constant

V : varied

collection of excess coating fluid was managed by fixing a collecting pipe to the pilot-plant coater as shown in Figure 11. Then, the excess amount of coating was collected in a container during 60 seconds. This procedure was repeated three times for each web speed. Finally, the average flow rate of the excess coating color (R_1) was calculated by dividing the mass of coating color collected in the container by the time interval as shown in Table 4. As a second step, the mass flow rate passing underneath



hw = Wet film thickness

m = Total mass flow rate

$R1$ = Mass flow rate of excess coating

$R2$ = Mass flow rate of coating passing underneath the blade

Figure 11. Collecting of Excess Coating Color.

Table 4
Determination of Excess Coating Flow Rate (R_1)

Speed (m/s)	1 st Run R_1 , (kg/s)	2 nd Run R_1 , (kg/s)	3 rd Run R_1 , (kg/s)	Average R_1 (kg/s)
3.07	0.446	0.443	0.445	0.445
4.00	0.511	0.516	0.511	0.513
4.95	0.705	0.702	0.706	0.704

the blade (R_2) was calculated from the coat weight. Thus, the total mass flow rate was determined at each web speed by adding these two figures (i.e., R_1+R_2) as shown in Table 5. The detailed procedures and the sample calculations for the determination of total mass flow rates are presented in Appendix B.

Table 5
Mass Flow Rates at Different Web Speeds

Speed (m/s)	Solids, %	R_1 (kg/s)	R_2 (kg/s)	m (R_1+R_2) (kg/s)
3.07	62.2	0.443	0.011	0.454
4.00	62.7	0.513	0.015	0.528
4.95	62.9	0.704	0.021	0.725

Incoming Layer Thickness

The major reason for keeping the mass flow rate

constant was to determine the incoming layer thickness of the coating color during the coating process. Since the overall mass flow rate of the coating color was constant, the incoming layer of coating color to the blade was calculated (see Appendix H) by using Equation 17.

$$h_1 = h_2 = \frac{m}{V * W * d} \quad [17]$$

where m = mass flow rate (kg/s),

V = web speed (m/s),

d = density of the suspension (kg/m³),

W = width of the paper web (m).

The incoming layer thickness was calculated for each web speed and results are shown in Figure 12.

Web Speed

During the coating trials, initially the coater speed was adjusted to achieve the desired constant web speed. Then, the coating color was applied with an applicator roll. However, in order to make sure that the web speed was the one that we had adjusted, the rotational speed of the backing roll was measured. Then the actual web speed was calculated (Table 6) and this number was used to calculate the prediction of each model. It was important to point out that the web speed was kept constant while coat weight data were obtained as a function of blade pressure.

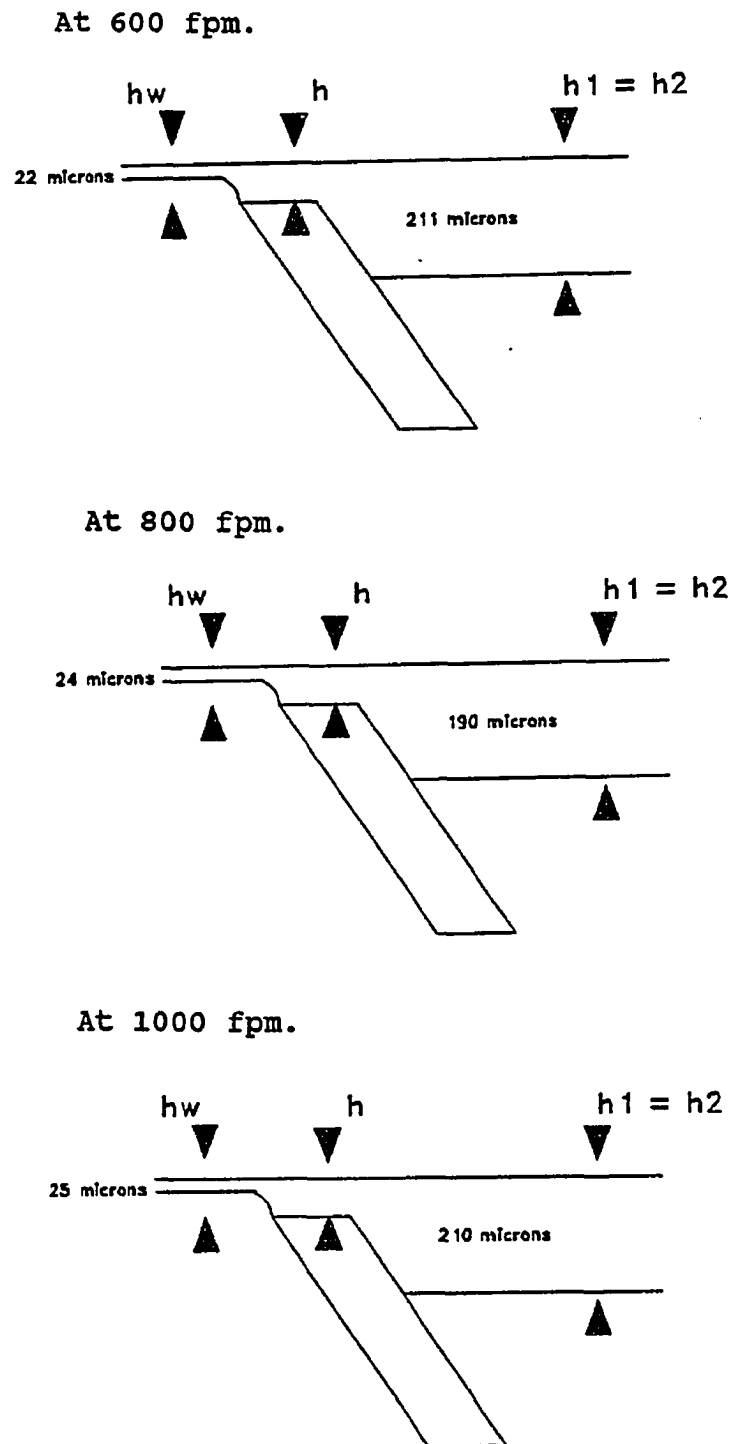


Figure 12. Incoming Layer Thickness (h_1) and Wet Film Thickness (h_w) at Each Web Speed.

Table 6
Actual Versus Adjusted Web Speeds

Adjusted Web Speed (fpm)	Actual Web Speed (fpm)
600 (3.05 m/s)	605 (3.07 m/s)
800 (4.06 m/s)	789 (4.00 m/s)
1000 (5.08 m/s)	975 (4.95 m/s)

Blade Type and Dimensions

The nominal thickness of the blade that was used was during the pilot-plant trials was 15 mils (381 microns). However, the actual thickness of the blade was measured at 20 different points. The average actual thickness of the blade was 400 microns. This value was used to calculate the prediction of each model. The determination of the actual thickness of the blade was important because the bevelled length of the blade was calculated depending on the thickness of the blade as shown in Equation 18.

$$s = \frac{c}{\sin\alpha} \quad [18]$$

where s = bevel length of the blade (μm),

c = thickness of the blade (μm),

α = blade angle.

This parameter, s , plays an important role when the prediction of models based on lubrication theory are calculated.

Blade dimensions were adjusted before the pilot-plant trials. The distance (X_1) (Figure 9, pp. 33) between the application point of the tube pressure to the tip of the blade (i.e., blade extension) was 1.0 inch. Because all of the proposed models and their equations were derived to predict the TDF at the tip of the blade, the corresponding tube pressure $(F_z)_{\text{critical}}$ had to be transferred to the tip of the blade. This was achieved by using Equation 19. The derivation of Equation 9 is presented in Appendix C.

$$F = \frac{1}{2} * F_z * \frac{X_3^2 (3X_1 + 2X_3)}{(X_1 + X_3)^3} \quad [19]$$

where F = Blade pressure at the tip of the blade (kPa),

F_z = Tube pressure (kPa),

X_1 = The distance from the application point of tube pressure to the tip of the blade (m),

X_3 = The distance from mounting of the blade to the application point of the tube pressure (m)

In order to derive Equation 19, the blade deflection was assumed to be zero. The reason was that $(\text{TDF})_{\text{exp}}$ was measured when the blade tube pressure was equal to TDF, in other words, when the net resultant force, F_o , exerted by

the blade onto paper was zero.

An interesting observation is that when the deflection of blade is assumed zero, the blade pressure transmission equation derived by Eklund and Kahila became as shown in Equation 20.

$$F = [1 + \frac{1}{2} * (\frac{X_1}{X_2})^3 - \frac{3}{2} * \frac{X_1}{X_2}] * F_z \quad [20]$$

This equation is mathematically equivalent to the equation that was derived in Appendix C (Equation 19). Therefore, (TDF)_{exp.} obtained from the experiments were converted to the corresponding force at the tip of the blade by using the conversion table shown in Table 7.

Blade Bevel Angle

All of the pilot-plant trials were conducted with a 45 degree angle of the bevel. The exact bevel angle was determined from photomicrographs (Figure 13) before and after experimental use. This investigation showed that while the new blade was initially 43 degrees, the angle was reduced about 2 degrees during the coating process. Blade angle photomicrographs also indicated that the blade ran on its toe during the coating process. The measured blade angle values were used in all calculations.

Table 7

Conversion Table to Determine
Pressure at the Tip of the Blade

X_2 (in)	X_3 (in)	X_1 (in)	Tube Pressure (psi)	Pressure at the Tip (psi)
2.5	1.5	1.0	6.0	1.83
2.5	1.5	1.0	7.0	2.14
2.5	1.5	1.0	8.0	2.44
2.5	1.5	1.0	9.0	2.75
2.5	1.5	1.0	10.0	3.05
2.5	1.5	1.0	11.0	3.36
2.5	1.5	1.0	12.0	3.67
2.5	1.5	1.0	13.0	3.97
2.5	1.5	1.0	14.0	4.28
2.5	1.5	1.0	15.0	4.58
2.5	1.5	1.0	16.0	4.89
2.5	1.5	1.0	17.0	5.19
2.5	1.5	1.0	18.0	5.50
2.5	1.5	1.0	19.0	5.80
2.5	1.5	1.0	20.0	6.11
2.5	1.5	1.0	21.0	6.41
2.5	1.5	1.0	22.0	6.72
2.5	1.5	1.0	23.0	7.03
2.5	1.5	1.0	24.0	7.33

Picture of the New Blade.



Picture of the Used blade.

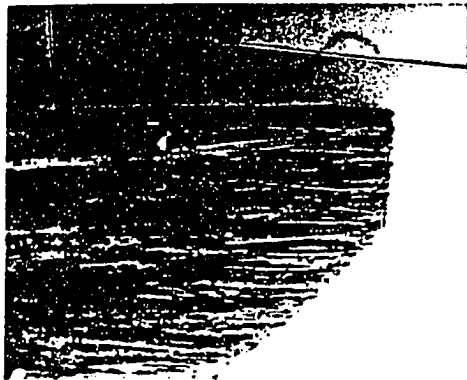


Figure 13. Photomicrographs of the Blade Before and After Use.

Coating Color Formulation

The coating formulation consisting of No. 1 clay, SB latex, and CMC was prepared at 62% solids. The following steps were followed in order to have a well-dispersed coating color. First, a 70% No. 1 clay dispersion was prepared and mixed about 40 minutes in a cowles dissolver. Then dilution water was added to reduce the solids percentage to about 65% and the dispersion was mixed 10 more minutes. Next, latex was added and mixed 15 minutes. Finally, CMC and dispersant were added gradually. Then coating was mixed 10 more minutes. Before the coating process was started, the actual solids level was measured and determined to be 61.7%. The actual temperature of the coating color was measured and recorded. Later, coating color viscosity was measured at the same temperature. The basic calculations and the procedure for the preparation of the coating is presented in Appendix D.

Absorption and Penetration Phenomena

All of the proposed equations to predict the TDF were derived assuming paper was nonabsorbent. This meant that the effects of fluid penetration and absorption into the web were neglected. In addition, the following assumptions were made in these analyses: (a) frictional losses were negligible, (b) velocity of the coating mass reaching to the blade was constant, (c) coating flow at the close

proximity of the blade was laminar, (d) coating fluid was incompressible, (e) blade could be considered as a cantilever beam, (f) for each different web speed, viscosity of the coating color was determined at only one shear rate, (g) incoming layer thickness (h_2) was assumed to be equal to the thickness of the coating color at the vicinity of the blade (h_1) (Figures 6 and 8), (h) the gap between the substrate and blade surface was assumed parallel, (j) elastic deformation was assumed for the blade, (l) compressibility of the paper, backing roll, and applicator roll were not considered, and (k) roughness of the substrate was considered only by Eklund and Kahila (2,16).

In this study, the models were tested by using the same assumptions as above. However, coat weight pickup is partially affected by penetration and absorption. In our case, coat weight data were obtained at maximum possible web speeds in order to reduce the dwell time and, accordingly, the penetration of continuous phase of coating color as well. However, the maximum web speed that could be achieved with the W.M.U. pilot-plant coater was 1000 fpm. A strategy was developed to avoid substantial penetration of the continuous phase of coating color into the web. These were:

1. A highly sized paper was obtained. The HST value (Hercules Sizing Tester) of the basesheet was measured at 85% reflectance by using no 2 ink. The HST values were 13

to 14 sec. Besides, base stock was supercalendered at 750 fpm and 1800 pli pressure. This process reduced surface roughness, compressibility and the absorptivity of paper. The average thickness of the roughness volume was measured, 1.8 microns, by using a profilometer. The compressibility of the basesheet was measured by using a parker print surf and the compressibility was 8%. The basesheet properties are summarized in Table 8.

2. The penetration of continuous phase into the paper web was reduced by preparing a coating color containing water retention agent, carboxymethylcellulose (CMC). It was assumed that the effect of these techniques would minimize penetration of the continuous phase of the coating color into the web. This assumption was checked by measuring the solids content of the coating color at each speed. The excess amount of coating was collected by fixing a pipe to the pilot-plant coater (Figure 11). This pipe prevented the recycle of the excess coating fluid striking at the edge of the blade. Therefore a coating fluid experiencing the dwell time by travelling with the paper web from the application point to the doctoring action of the blade was collected for each web speed. These coating samples were used for the determination of both actual solid level and the viscosity of coating color. Solids level and percent solids increase are presented in Table 9. Based on results, the solid percent

Table 8
Basesheet Properties

Furnish	35/65 (SW/HW)
Filler	14 % CaCO ₃ and 5 % Clay
Sizing, Internal	5 Ib AKD/T
Sizing, Surface	Starch
Basis Weight	92.2 g/m ²
Moisture	5.0 - 5.5 %
HST at % 85 Ref.	13 - 14 sec.
Opacity	92 %
Brightness	81 %
Caliper	91 um
Ash at 500 °C	19 %
Compressibility at PPS	8 %
Roughness thickness	1.8 um

increase was a maximum of 0.8% when the web speed was minimum (600 fpm). Therefore, the penetration of continuous phase into the paper web can be considered negligible.

Viscosity of Coating Color

The basic assumption in all of the previous analyses to determine the coating color viscosity was that there was only one fixed shear rate both underneath and at the vicinity of the blade tip. In this study, the coating

Table 9
Solid Contents of Coating Color

Speed (fpm)	Initial Solids at the Pond, %	Solids at the Blade, %	Solids % Increase,
600	61.7	62.2	0.8
800	62.2	62.7	0.6
1000	62.7	62.9	0.5

color viscosity was measured at each web speed under the same assumption. Viscosity data (Figure 14) were obtained by using the Hercules hi-shear viscometer (HHSV). Rheograms indicated that the steady shear viscosity increased from 10 cps at $10,000 \text{ sec}^{-1}$ to about 15 cps at $130,000 \text{ sec}^{-1}$. These measurements were obtained within a two second ramp time. Thus, interferences from viscous heating were minimized.

In order to calculate the predictions of existing models, shear viscosity values both underneath and at the vicinity of the blade tip were determined. Since the $(\text{TDF})_{\text{exp}}$ was experimentally determined at 600, 800, and 1000 fpm, the corresponding shear rates were calculated and the shear viscosity values were determined at the corresponding shear rates. For each web speed, the corresponding shear rate and the viscosity data are listed in Table 10.

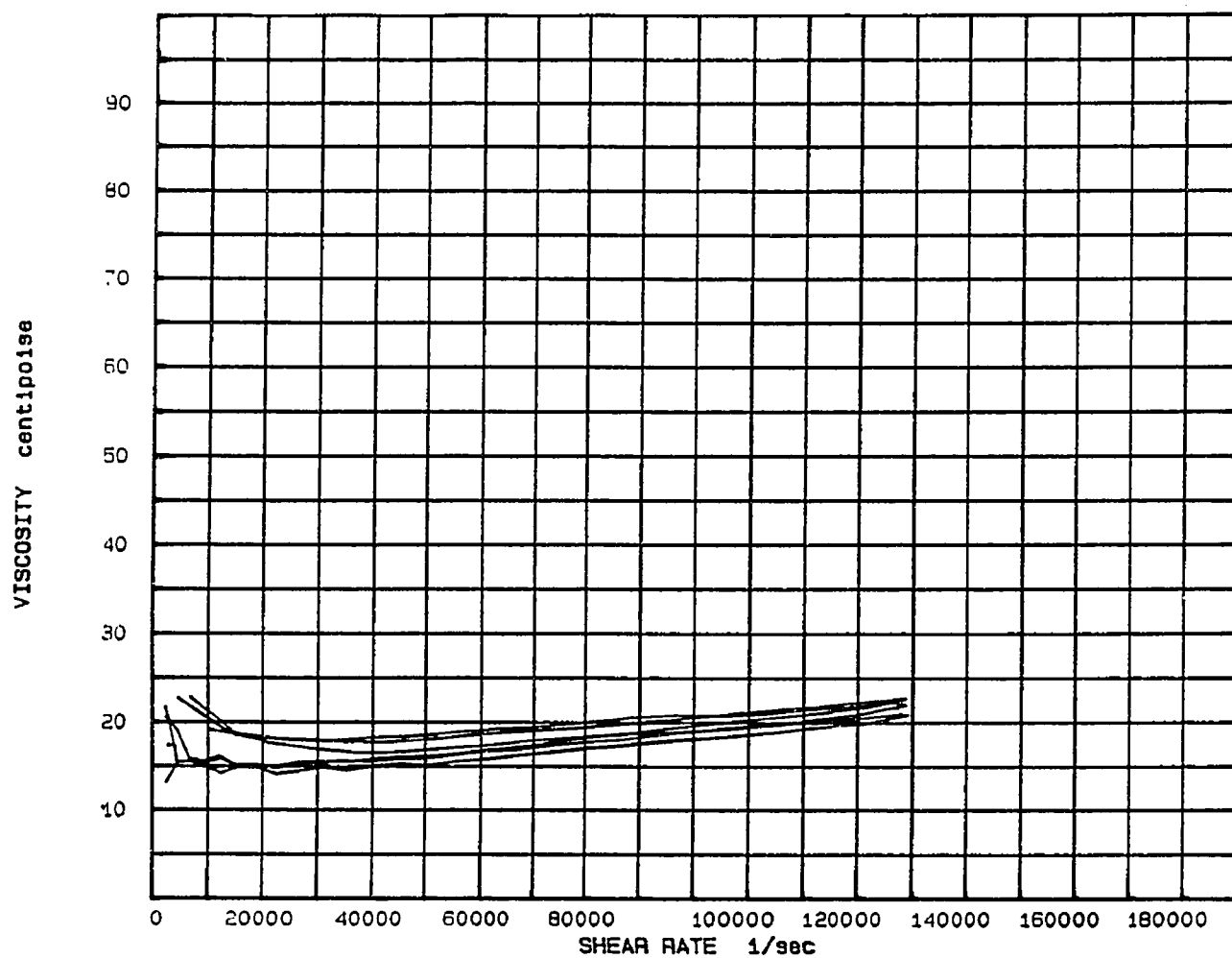


Figure 14. Viscosity of Coating Color.

Table 10
Viscosity Values at Each Web Speed

Speed (fpm)	Shear Rate at Vicinity (sec ⁻¹)	Viscosity at Vicinity (Cps)	Shear Rate the Tip (sec ⁻¹)	Viscosity the Tip (Cps)
600	14,500	12	109,000	16
800	19,000	13	127,000	17
1000	23,500	14	145,000	19

CHAPTER VIII

EXPERIMENTAL RESULTS AND DISCUSSION

First Pilot-Plant Trial

Based on the previous analyses when web speed, under constant blade load, is increased starting at very low speeds, coat weight diminishes and eventually reaches a minimum value. At this point the corresponding speed is termed the critical web speed. The reason for decreasing coat weight is that coat weight is affected by absorption and penetration when web speed is lower than the critical web speed. However, when the web speed exceeds the critical speed then the coat weight starts increasing. This indicates that, dynamic forces become dominant.

The main objective of this research was to evaluate the existing equations describing the dynamic forces generated by coating color. Therefore, trials were conducted at coating speeds above critical web speed.

The maximum web speed that could be achieved in the pilot-plant coater was 1000 fpm. It was unknown whether web speeds between 500 to 1000 fpm were greater than the critical web speed. Therefore, the first trial was conducted to document that the selected web speeds were greater than the critical web speed. The pilot-plant

coater was run at constant blade pressure of 25 psi and coat weight data were obtained at three different web speeds.

Results (Figure 15) indicated that coat weight increased as the web speed was increased from 500 to 1000 fpm. These results verified that dynamic forces were dominant within this range of web speeds. Therefore, the existing equations, derived to predict TDF for the bevelled blade coater, could be tested. The data for the first pilot-plant trial are presented in Appendix E.

Second Pilot-Plant Trial

This pilot plant trial was done at three different web speeds after proving that dynamic forces were dominant within selected web speed ranges. Coat weight data were obtained by changing the blade pressure at constant web speed. The first set of data were obtained by running the coater at 500 fpm. Coat weight was obtained first at maximum blade pressure (45 psi), then additional data were obtained by reducing the blade pressure. During the trials, the blade pressure was reduced to the point where it was lower than the $(TDF)_{exp.}$, i.e., there was no net resultant force exerted onto the blade and paper web, so that blade detached from the paper web and accordingly coat weight increased suddenly. The same procedure was repeated to obtain the second and third sets of coat weight

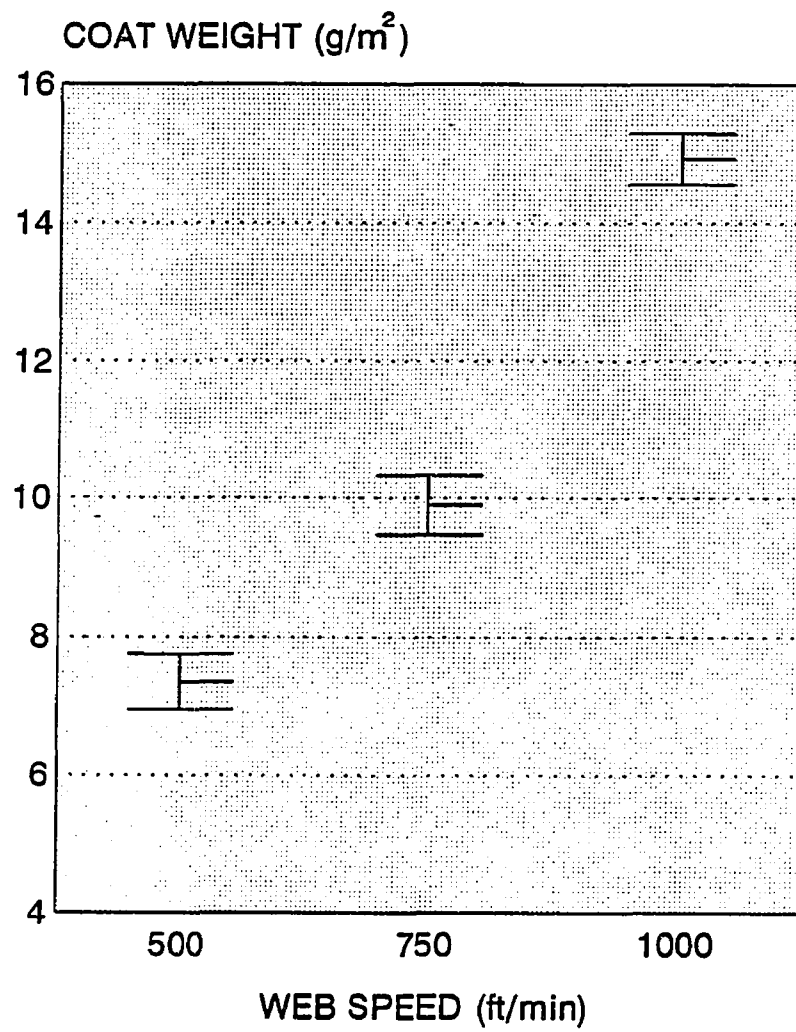


Figure 15. Coat Weight Versus Web Speed.

data as a function of blade pressure at 750 and 1000 fpm. The coat weight versus blade pressure graphs were drawn at each web speed as shown in Figures 16, 17, and 18. From this information, narrower blade pressure ranges which were about equal to the $(TDF)_{exp.}$ for each web speed were selected. These ranges were 10 to 20 psi at 500 fpm; 15 to 25 psi at 750 fpm; and 20 to 30 psi at 1000 fpm. Details of the experimental data from this trial are presented in Appendix F.

Third Pilot-Plant Trial

Experimental conditions similar to the second trials were repeated within the narrower blade pressure ranges, but web speeds were 600, 800, and 1000 fpm. The goal was to determine the corresponding $(TDF)_{exp.}$ at each web speed. Therefore, additional coat weight data were obtained while the blade pressure was reduced by one psi decrements at each web speed. As a result, coat weight versus blade pressure graphs (Figures 19-21) were drawn to determine the corresponding $(TDF)_{exp.}$ at 600, 800, and 1000 fpm. Details of the experimental data for the third trial are presented in Appendix G.

Determination of Dynamic Forces

At 600 fpm

The coat weight increased gradually from 6.9 to 15.4

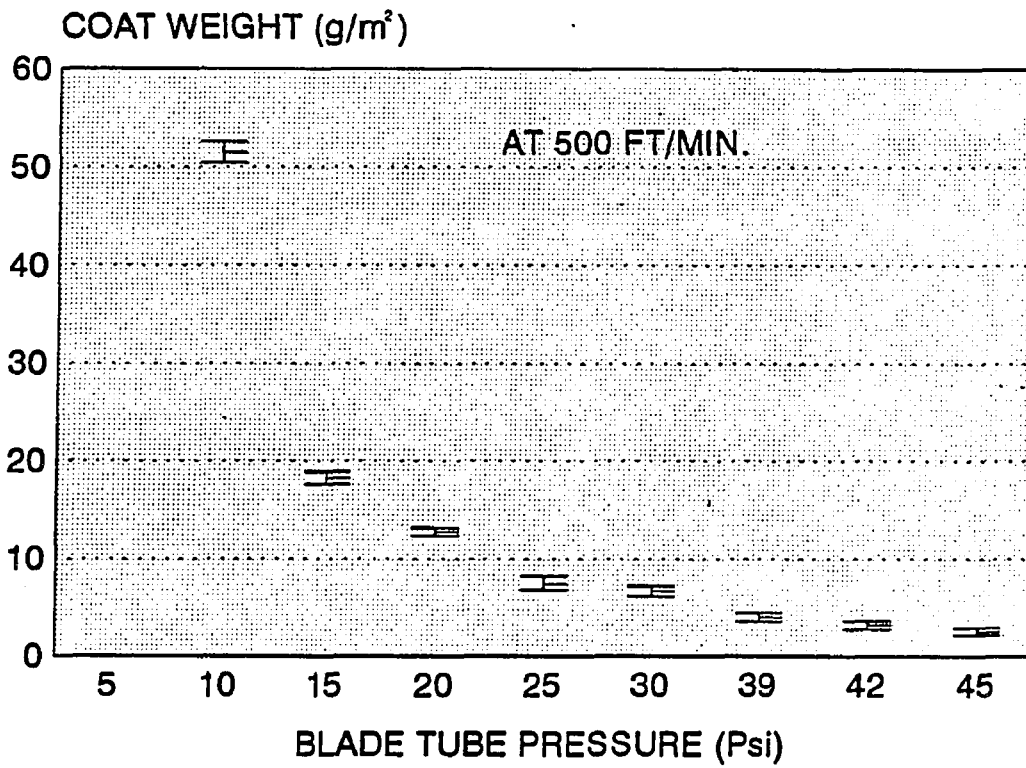


Figure 16. Coat Weight Versus Blade Pressure at 500 fpm.

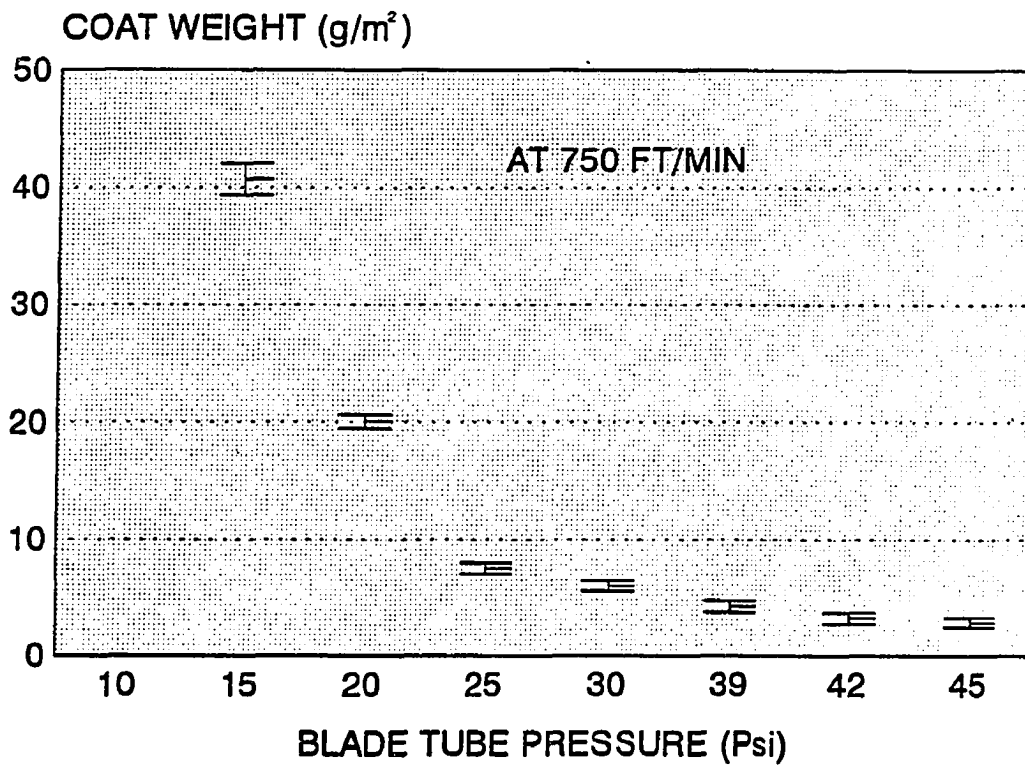


Figure 17. Coat Weight Versus Blade Pressure at 750 fpm.

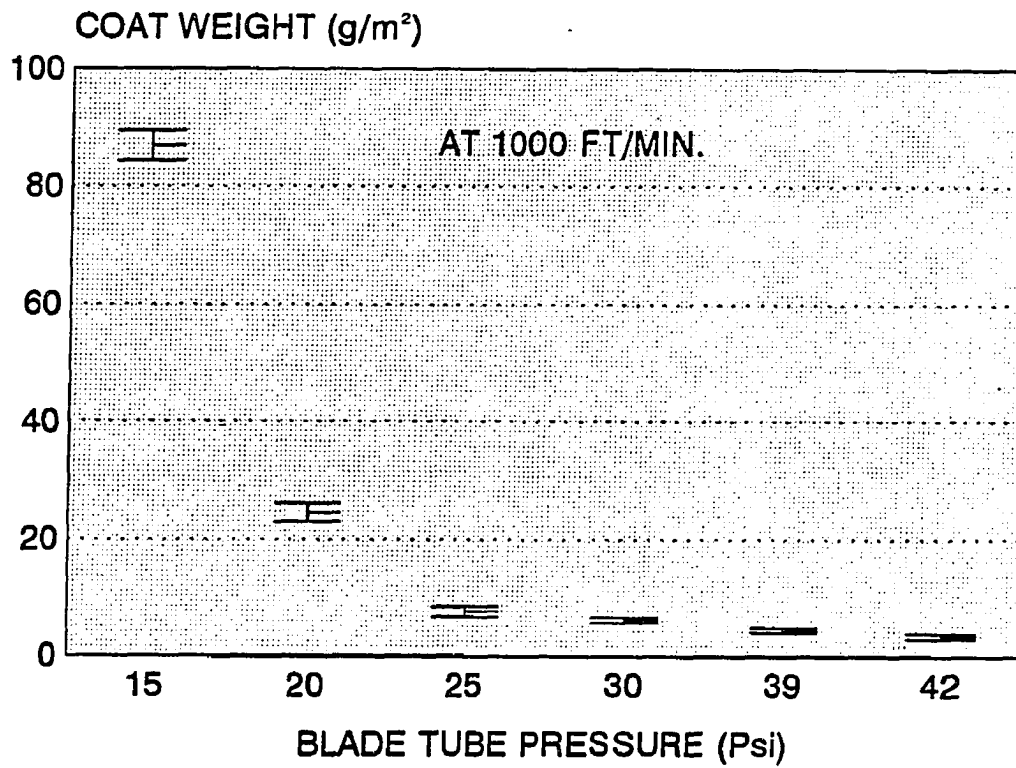


Figure 18. Coat Weight Versus Blade Pressure at 1000 fpm.

g/m^2 while the blade tube pressure was decreased from 22 to 12 psi, as shown in Figure 19. The reason was that the blade tube pressure was greater than $(\text{TDF})_{\text{exp}}$ when it was in between 22 to 12 psi so that coat weight was controlled by net resultant force exerted onto the blade and paper web. However, coat weight increased abruptly from 15.4 to 34.5 g/m^2 when the blade pressure was decreased from 12 to 10 psi (Figure 19). This dramatic coat weight increase indicated that TDF exceeded the blade load when it was reduced below 12 psi. As a result, $(\text{TDF})_{\text{exp}}$ at 600 fpm was greater than 10 psi but smaller than 12 psi.

At 800 fpm

With the same technique, the coat weight data were collected as a function of blade pressure at 800 fpm. Blade tube pressure was reduced from 25 psi to 14 psi and coat weight data was determined at each blade pressure (Figure 20). Experimental results indicated that the coating process was stable while the blade tube pressure was reduced from 25 to 17 psi. It is clearly shown in Figure 26 that coat weight increased gradually when the blade tube pressure was reduced from 25 to 17 psi. However, when the blade pressure was decreased from 17 to 16 psi, coat weight increased dramatically. The reason for the 21.1 g/m^2 increase in coat weight with only one psi reduction at blade tube pressure was that $(\text{TDF})_{\text{exp}}$.

exceeded the blade tube pressure so that the blade was detached from the paper and the process became unstable. As a result, it was concluded that $(TDF)_{exp.}$ at 800 fpm was smaller than 17 psi but greater than 16 psi.

At 1000 fpm

Coat weight data was obtained first at 35 psi then more data were generated by reducing the blade tube pressure to 21 psi. Coat weight increased gradually when the blade tube pressure was reduced from 35 to 23 psi as shown in Figure 21. However, coat weight increased rapidly from 11.0 g/m^2 to 19.4 g/m^2 when the blade pressure was decreased from 23 to 22 psi. This abrupt change in coat weight indicated that $(TDF)_{exp.}$ was greater than 22 and smaller than 23 psi.

As a result of the pilot-plant trials, $(TDF)_{exp.}$ at each web speed was experimentally determined in terms of narrower blade tube pressure ranges as shown in Table 11. The measured tube pressure was converted to the corresponding TDF at the tip of the blade (also presented in Table 11). These values were used to compare the experimental data with the prediction of the models.

Comparison of Experimental Results With the Models

The equations of the various models were solved under the experimental conditions at each web speed. In parti-

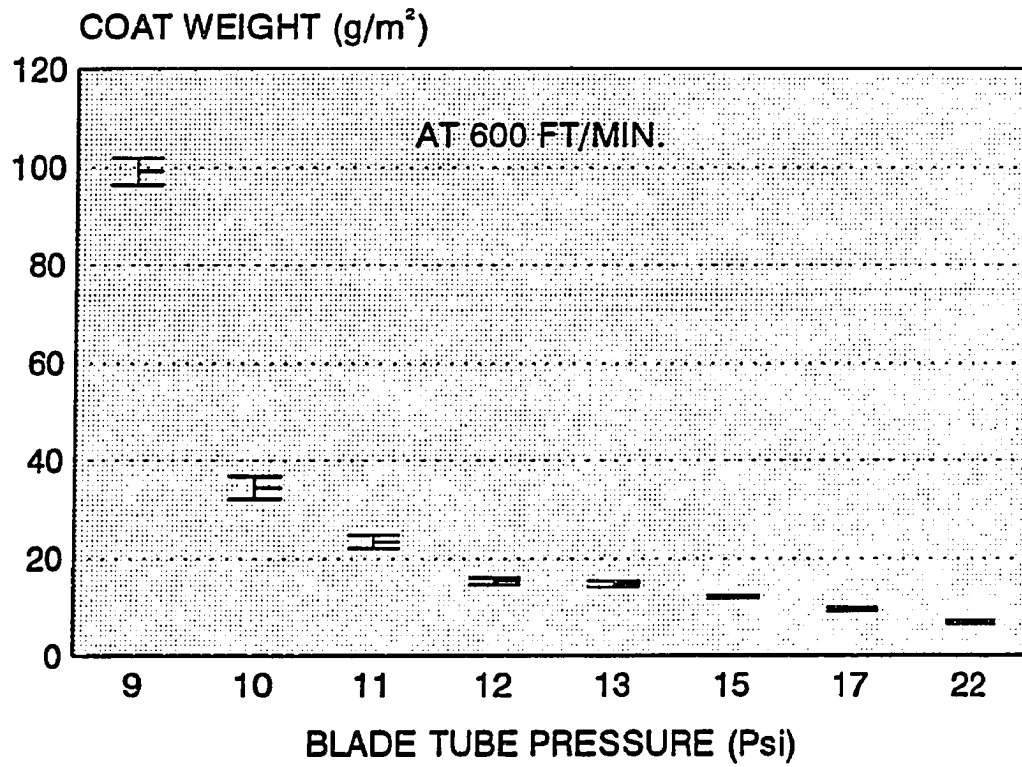


Figure 19. Coat Weight Versus Blade Pressure at 600 fpm.

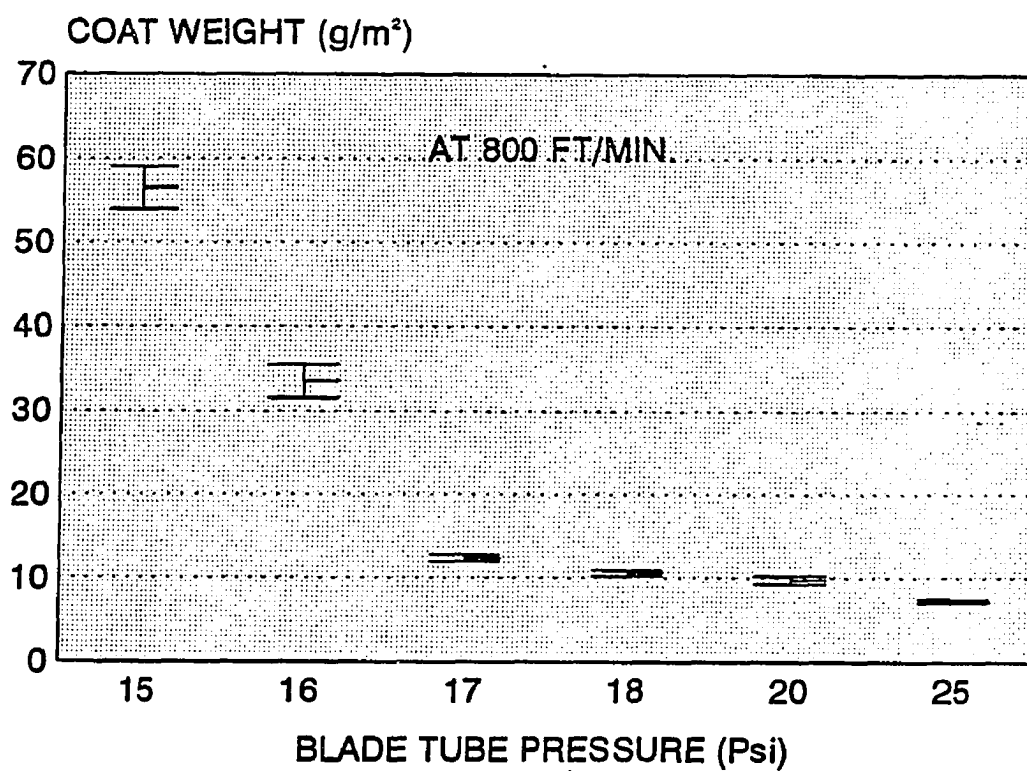


Figure 20. Coat Weight Versus Blade Pressure at 800 fpm.

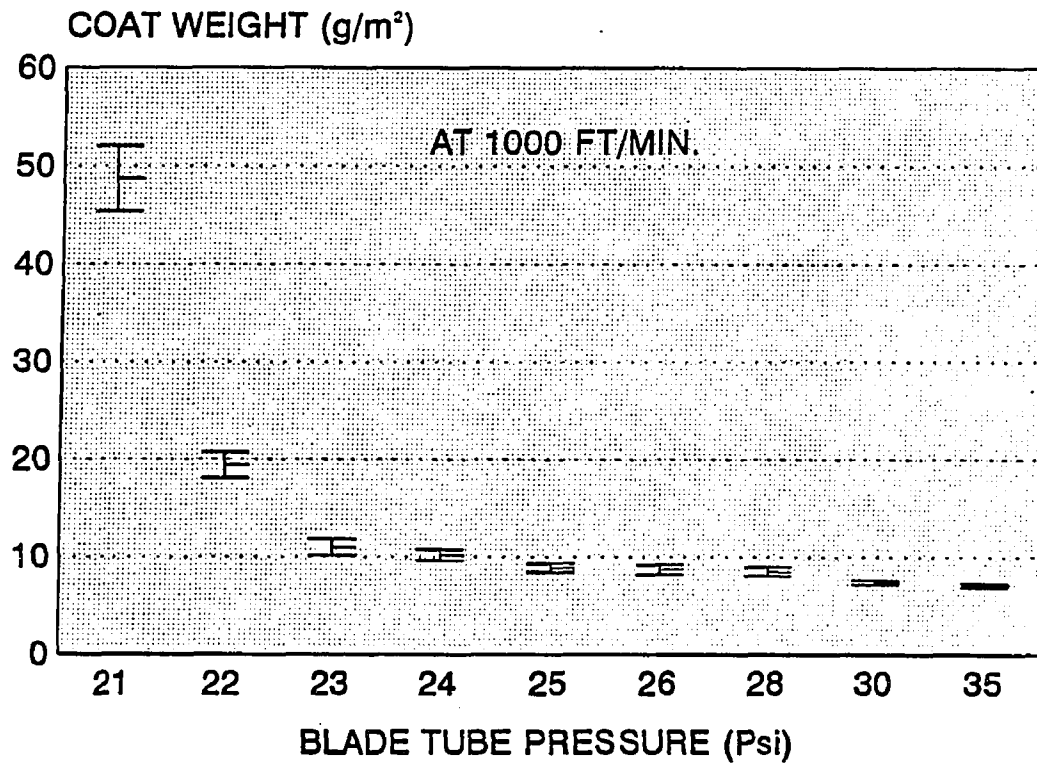


Figure 21. Coat Weight Versus Blade Pressure at 1000 fpm.

Table 11
Total Dynamic Forces at Each Web Speed

Speed (fpm)	(TDF) _{exp.} as a Tube Pressure (psi)	(TDF) _{exp.} at the Blade Tip
600	10 < (TDF) < 11	3.05 < (TDF) < 3.36
800	16 < (TDF) < 17	4.89 < (TDF) < 5.19
1000	22 < (TDF) < 23	6.72 < (TDF) < 7.03

cular, (TDF)_{calc.} for each model was calculated and compared with the experimental results, i.e., the magnitude of (TDF)_{exp.} Following is the presentation of comparisons between the measured values of TDF with the calculated value of the TDF.

Prediction of Lubrication Theory

The hydrodynamic pressure underneath the blade tip was calculated by substituting measured parameters during the experimental trials into Equation 8 (3).

$$F_{hy} = \frac{6\mu s^2 V}{h_o^2} \left(1 - \frac{2h_w}{h_o}\right) \quad [8]$$

where F_{hy} = Hydrodynamic force per unit length (N/m)

s = the length of bevelled surface (um),

h_o = the coating thickness experiencing shear (um),

h_w = the thickness of the wet coating (um),

μ = coating color viscosity (kg/m-s),

V = web speed (m/s).

There was a major difficulty in calculating the hydrodynamic pressure based on Equation 8. That was the estimation of the magnitude of effective thickness, h , which is experiencing the highest shear and lying in between the paper web and the surface of the blade (Figure 4). During the coating process, the exact value of h at each speed was unknown because of the complexity of the process. In general, differential thickness of coating color will be present at various regions because the web surface is rough, nonuniform, and compressible. Particularly, the coating thickness would be greater at the "valleys"--regions in between fiber crossings at the web surface--than at the "hills"--areas where fiber crossing or overlapping exists. Such variations of coating thickness would induce spatial variations in shear. Since the coating color considered here is shear thickening, the flow rate at the blade tip would also vary depending on the surface morphology of the web.

Spatial variability of coating coverage has been controlled in these experiments by minimizing web roughness and compressibility. The average thickness of the roughness volume was 1.8 microns and the compressibility of the base stock was 8%.

Although there was a spatial variation of the wet

film thickness, h_0 , under the blade tip, the range within which the average thickness varied can be estimated. This value lies between the thickness of the incoming coating layer, h_1 , and the thickness of the wet coating deposited onto the web, h_w . Thickness h_1 is the layer of coating travelling with the web in the region between the applicator roll and blade. It was shown earlier that dewatering via transport of the continuous phase from the coating into the porous web was minimal, i.e., at most less than 0.8% (Table 9). Thickness of the gap, h , has to be in between h_1 and h_w ; h_1 representing the maximum and h_w a minimum value. The calculated values of both h_1 and h_w at each web speed are given in Figure 12. Therefore, even though the exact value of the effective gap was not known, the upper limit, h_1 , and the lower limit, h_w , for the effective gap were known at each web speed as shown in Table 12.

The hydrodynamic pressures, based on Equation 8, were calculated for different h_0 values in between the maximum and minimum values of h_0 at each web speed. The calculated results (Figures 22-24) indicated that the hydrodynamic pressure, as a function of h_0 , initially increases with increasing h up to a point then it decreased with further increases in the value of h . The maximum pressure becomes larger with increasing web speed (Table 13) because the hydrodynamic pressure in Equation 8 is directly related

Table 12
Determination of Upper and Lower Limits
for the Effective Gap

Speed (fpm)	Upper Limit h_1 (microns)	Lower Limit h_w	Effective Gap h_o
600	211	22	$22 < h_o < 211$
800	189	24	$24 < h_o < 189$
1000	210	25	$25 < h_o < 210$

with the web speed.

Table 13
Determination of Maximum Hydrodynamic Pressure
Underneath the Blade Based on Lubrication Model

Speed (fpm)	h_{max} (mic)	(TDF) _{calc} (psi)	(TDF) _{exp.} (psi)
600	60	1.5	3.10 ± 0.20
800	70	1.7	5.00 ± 0.10
1000	80	2.1	6.85 ± 0.15

Additionally, the corresponding gap value at the maximum hydrodynamic pressure is higher at greater web speeds, i.e., about 60 microns at 600 fpm and about 80 microns at 1000 fpm. The reason is when the web speed is increased, the magnitude of TDF acting on the blade will increase. As a result, the net resultant force exerted onto the blade decreases, and, accordingly, the blade will

rise more from the paper web, therefore, the effective gap becomes higher. Consequently, even though the actual value of h was not known, Figures 22-24 demonstrate that even at the maximum pressure the calculated values were considerably less than the measured values for TDF. Therefore, when experimental results are compared with the predictions of the lubrication model, hydrodynamic lubrication cannot explain coat weight development. This is true even though the experimental results are compared with the maximum possible pressure at each web speed, as shown in Table 13. These results indicated that the calculated hydrodynamic pressure underneath the blade can be at maximum 34% of the TDF at 800 fpm and 31% of the TDF at 1000 fpm. It seems that lubrication is quantitatively more important at low speeds than high speeds. In all cases investigated, however, the maximum hydrodynamic lift underneath the blade did not account for more than 50% of the $(TDF)_{exp.}$. Therefore, it is concluded that the hydrodynamic force was not sufficient to explain the coat weight development under the conditions investigated in this study. The sample calculations are presented in Appendix I.

Prediction of the Impact Model

According to this model, the TDF acting on the blade is defined as the summation of the impulse, pressure, and

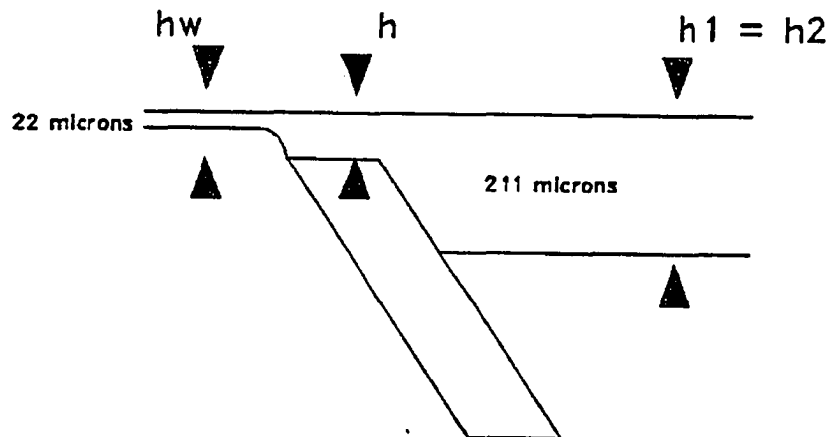
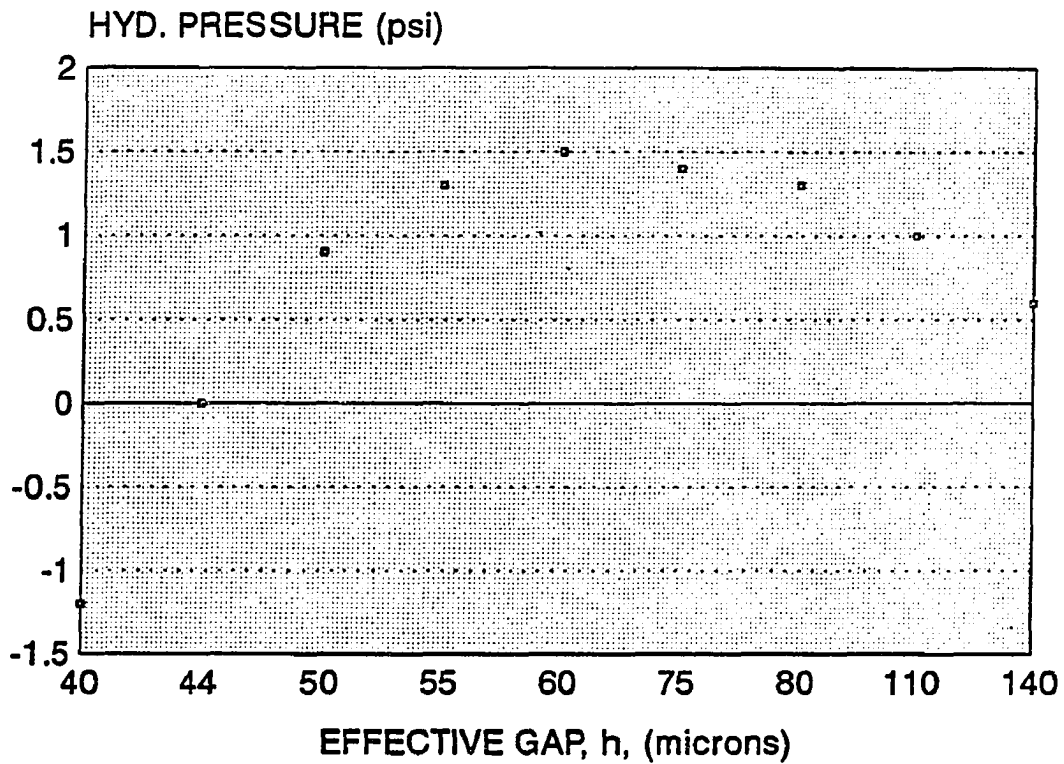


Figure 22. Hydrodynamic Lubrication Force as a Function of the Effective Gap at 600 fpm.

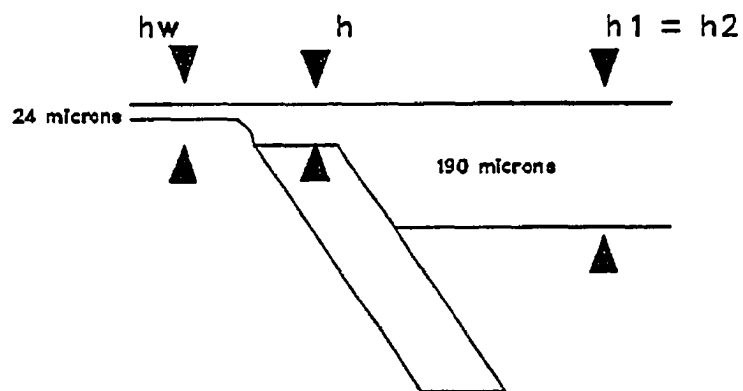
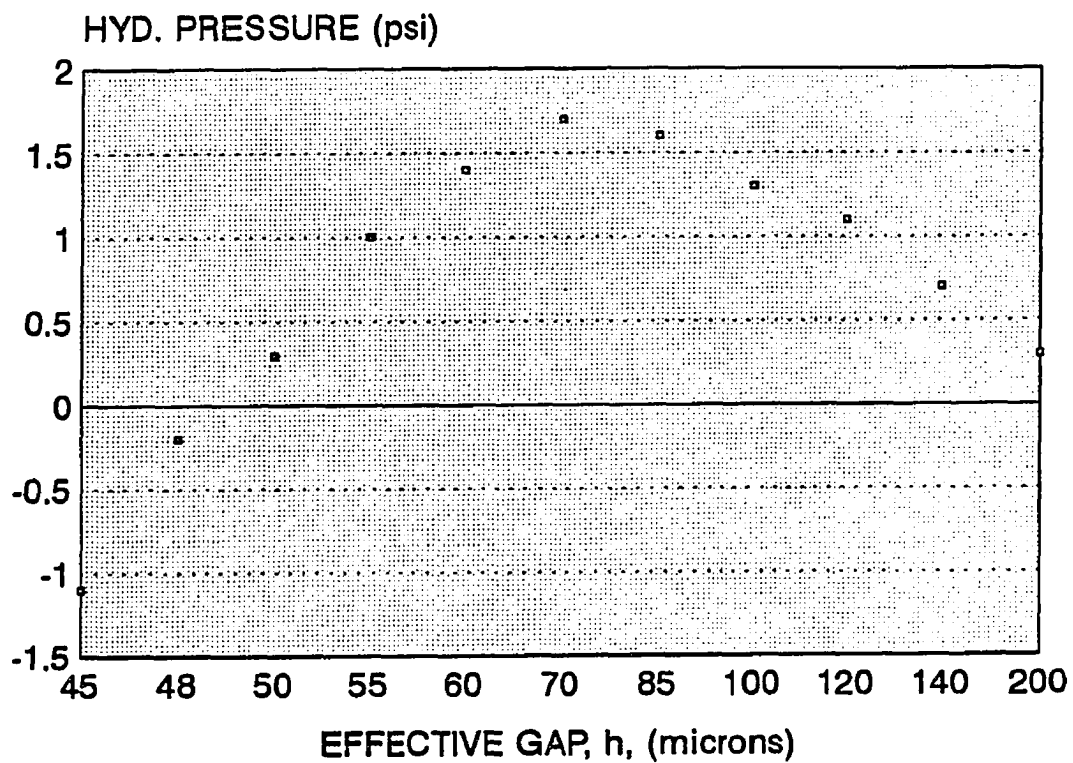


Figure 23. Hydrodynamic Lubrication Force as a Function of the Effective Gap at 800 fpm.

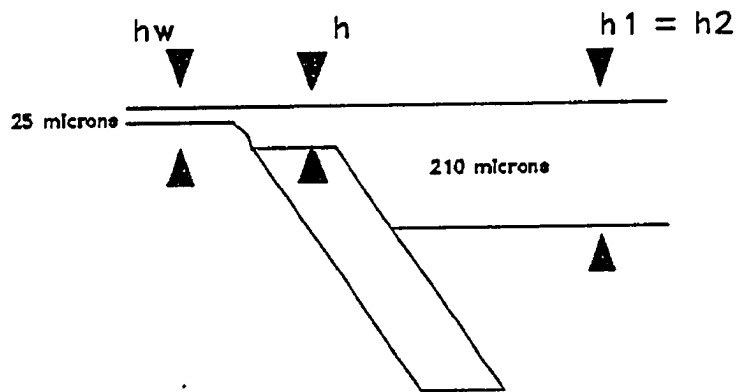
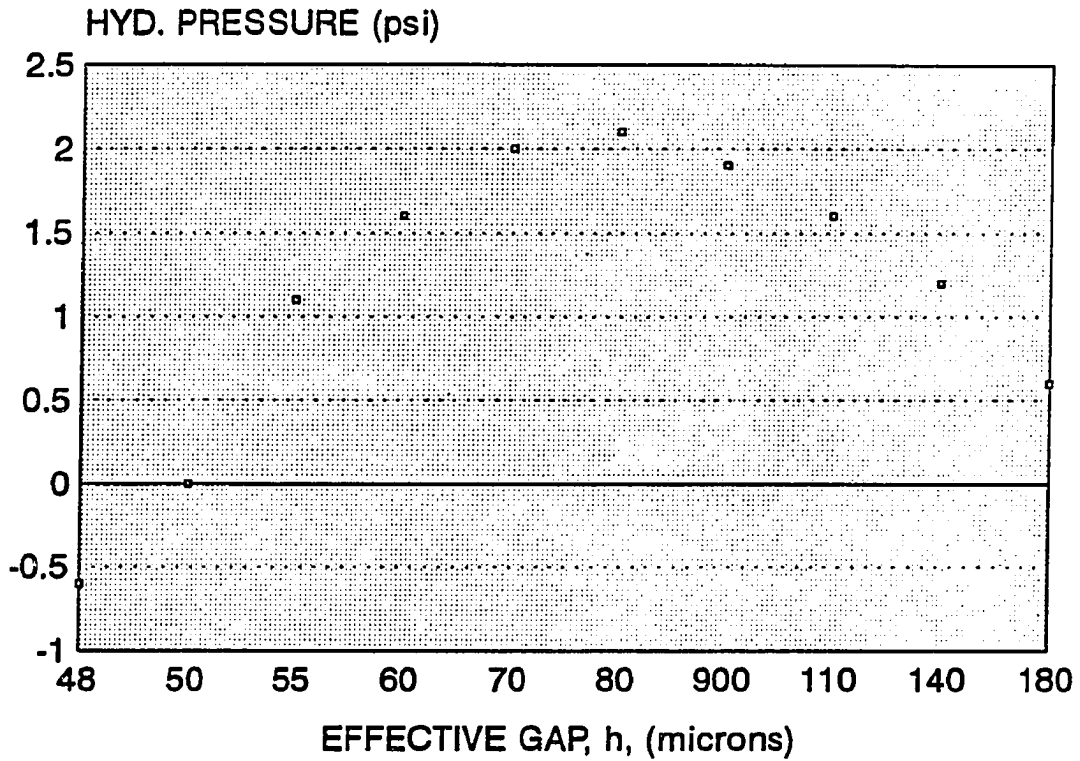


Figure 24. Hydrodynamic Lubrication Force as a Function of the Effective Gap at 1000 fpm.

hydrodynamic forces. Predictions of each individual dynamic force, based on this model, have been calculated and results are presented in Table 14. Sample calculations are presented in Appendix J.

Table 14
Prediction of Dynamic Forces According to
Impact Model at Each Web Speed

Speed (fpm)	Impulse (psi)	Pressure (psi)	Hydro. at the Proximity of Blade (psi)	(TDF) _{calc.} (psi)
600	2.8	2.1	0.2	5.1
800	4.8	3.7	0.2	8.7
1000	6.8	5.1	0.2	12.1

When the calculated and measured TDF are compared, it can be seen that (TDF)_{calc.} exceeds (TDF)_{exp.} at each web speed (Table 15). The calculated values are 65 to 75% higher than the measured TDF values (Table 15), the greater difference corresponding to higher web speed. The magnitude of TDF was determined at a narrower range at each web speed, therefore there is an uncertainty in estimating the exact value of the (TDF)_{exp.}. The uncertainty was 6% at 600 fpm and 2% at 1000 fpm and these uncertainties were significantly lower than the difference between the calculated and measured values. Therefore, experimental results indicated that the momentum change of excess

coating color had been counted twice in this analysis by considering both impulse and pressure force. Consequently, the impact model, as originally developed by Kahila and Eklund (2), could not quantitatively predict coat weight development when it was considered as a summation of three dynamic forces, as shown in Table 15.

Table 15

Comparison Between Experimentally Measured TDF
and Calculated TDF According to Impact Model

Web Speed (fpm)	(TDF) _{calc.} (psi)	(TDF) _{exp.} (psi)
600	5.1	3.10 ± 0.20
800	8.7	5.00 ± 0.10
1000	12.1	6.85 ± 0.15

In contrast, when the TDF acting on the blade was calculated as the summation of only two forces, i.e., the impulse and hydrodynamic force, the predictions of the impact model were in good agreement with the experimental findings because (TDF)_{calc.} and (TDF)_{exp.} are almost the same at each web speed (Table 16).

These results support the argument that the force for the momentum change of the excess coating was considered twice in the original development of the impact model. For that reason, there were excess forces when the TDF was calculated (Table 14) as a summation of three forces.

Table 16

Predictions of Impact Model as a Combination of
Impulse and Hydrodynamic Forces at Each Web Speed

Speed (fpm)	Impulse (psi)	Hydrodynamic (psi)	(TDF) _{calc.} (psi)	(TDF) _{exp.} (psi)
600	2.8	0.2	3.0	3.10 ± 0.20
800	4.8	0.2	5.0	5.00 ± 0.10
1000	6.8	0.2	7.0	6.85 ± 0.15

Another important conclusion was that while the hydrodynamic force accounted for 7% of the TDF at 600 fpm, it was only 3% of the TDF at 1000 fpm. It should be pointed out that the hydrodynamic force in the impact model represents the hydrodynamic lift at the underside of the blade not underneath the blade as in lubrication model. Therefore, the impulse force could be considered the primary force controlling the coat weight development during bevelled blade coating process. The effect of the impulse force is greater as machine speed rises.

Combination of Impulse and Hydrodynamic Force

This model, proposed by Kuzmak (4), suggests that the TDF can be calculated from the summation of the impulse force and hydrodynamic force underneath the blade. Kuzmak's pilot-plant trials showed that the hydrodynamic lift underneath the blade was the dominant force in bevel-

led blade coating.

When the TDF was calculated according to Kuzmak's approach for the data obtained in this study, the results indicated that the prediction of his model exceeded $(TDF)_{exp}$. about 1.2 to 3.0 psi depending on web speeds as shown in Table 17. This excess amount of calculated force might be due to the use of the maximum possible hydrodynamic force during the calculations. This model may predict the TDF if the exact value of the hydrodynamic force were known. In reality the hydrodynamic force based on lubrication theory is expected to be smaller than its maximum value at each web speed (Figures 22-24). Based on the calculations by considering maximum hydrodynamic lift, the predictions of Kuzmak's approach was comparable to the experimental TDF (Table 17). The important observation was that even though this model gave results comparable to the experimental findings, the main force controlling coat weight development was not the hydrodynamic force, as Kuzmak concluded, but the impulse force. The sample calculations are presented in Appendix I and J.

Lateral Force Model

All of the existing analyses considered up to now assumed that the lateral (or shear) force both underneath and at close proximity to the blade were too small to be considered in the force balance. Kartovaara (5) has

Table 17

Combination of Impulse and Hydrodynamic Lubrication
Forces at Each Web Speed

Speed (fpm)	Impulse (psi)	Hydrodynamic Under the Blade (psi)	(TDF) _{calc.} (psi)	(TDF) _{exp.} (psi)
600	2.8	1.5	4.3	3.10 ± 0.20
800	4.8	1.7	6.5	5.00 ± 0.10
1000	6.8	2.1	8.9	6.85 ± 0.15

recently considered this force and derived an equation to calculate it (Equation 6). The critical parameter in his equation was the thickness of the roughness volume. This parameter for the paper used in this study was measured by using profilometer. The roughness thickness was 1.8 microns. Results (Table 18) indicated that the lateral force was about 7% of the TDF at 600 fpm and only 6% of the TDF at 1000 fpm.

Table 18
Corresponding Lateral Force at
Each Web Speed

Speed (fpm)	Lateral (psi)	(TDF) _{exp.} (psi)
600	0.20	3.10 ± 0.20
800	0.30	5.00 ± 0.10
1000	0.40	6.85 ± 0.15

CHAPTER IX

CONCLUSIONS

Pilot-plant data have been compared with the proposed models of the bevelled blade coating process for paper webs. The case that has been investigated minimized the effect of web absorbency and compressibility. Under these conditions, it has been concluded that:

1. The calculated results, based on lubrication theory indicated the hydrodynamic pressure underneath the blade could be at maximum 48% of TDF at 600 fpm, 34% of TDF at 800 fpm, and 31 % at 1000 fpm. Therefore, the total dynamic forces could not be explained with only hydrodynamic lubrication theory. This was true even though experimental results were compared with the maximum possible hydrodynamic pressure at each web speed. As a result, the hydrodynamic force was not the primary force controlling the coat weight development during the coating process.

2. Experimental results indicated that the momentum change of excess coating color has been counted twice in the impact model by considering both impulse and pressure forces. Therefore, the $(TDF)_{calc}$ exceeded $(TDF)_{exp}$. at each web speed.

3. The impact model could predict coat weight development at each web speed when it was considered as a summation of only the impulse and hydrodynamic force (i.e., when hydrodynamic force was considered at the vicinity of the blade tip). The hydrodynamic force, in this model, accounted for only about 6% of the $(TDF)_{exp.}$, while the impulse force represented 94% of the $(TDF)_{exp.}$

4. While the combination of impulse and hydrodynamic force (i.e., the hydrodynamic lift underneath the blade) generated the second most reliable predictions, results indicated that: (a) the primary force controlling coat weight development was not a hydrodynamic force, as Kuzmak concluded, but impulse force, and (b) results indicated that since the hydrodynamic force was not a primary force it did not make much of a difference whether the hydrodynamic force was considered underneath the blade or at the close vicinity of the blade.

5. Results in this research were not in agreement with the assumption that lateral force was too small to be considered in a force balance around the blade tip. Experimental results indicated that lateral force was about 7% of the TDF at 600 fpm and 6% of the TDF at 1000 fpm, while the hydrodynamic force in the impact model was about 6% of the TDF. Therefore, this force should not be neglected since it is roughly the same magnitude as the hydrodynamic force at the proximity of the blade.

6. Since all of the existing equations were derived as if paper was nonabsorbent, there was a linear relationship between the operational parameters and the results of each equation tested in this study. The general observation was when the web speed was increased, the quantitative value of the hydrodynamic force increased. However, the percentage hydrodynamic force within TDF was diminished regardless of whether it was considered underneath or at the vicinity of the blade. The same results were observed for the lateral force. The reason was that when the web speed was increased, two important parameters were affected. The first one was the viscosity, the second one was the mass flow rate of the coating color. Both of these parameters increased quantitatively when the web speed was increased. While a quantitative increase in the mass flow rate greatly affected the impulse force, the quantitative increase in the hydrodynamic force was minor compared to the change in the impulse force. Therefore, in the cases investigated, mass flow rate of the coating color was the critical parameter to control coat weight development, not the viscosity of the coating color.

APPENDICES

Appendix A

Derivation of the Hydrodynamic Force Based on Lubrication Theory

In fluid dynamics, the goal is to find the velocity distribution as well as the state functions of the fluid at any point in space, for all time. There are six unknowns: The three velocity component u , v , w , temperature T , and pressure P , and the density ρ of the fluid, which are all functions of the spatial coordinates x , y , z , and time t .

In order to determine the six unknowns, six relationships are needed to connect them. These are:

1. The equation of state, which connects the temperature, pressure, and density of the fluid.
2. The equation of energy, which expresses the conservation of energy of the fluid.
3. The equation of continuity, which expresses the conservation of mass of the fluid.
- 4-6. The Navier-Stokes equations, which correspond to Newton's three equations of motions in fluid dynamic.

The mathematical form of these six relationships for the particular situation:

1. It is assumed that the coating fluids are incompressible liquids, the equation of state is:

$$\rho = \text{constant}$$

2. It is assumed that the temperature of coating color is in equilibrium with the surroundings so that energy equation is reduced to:

$$T = \text{constant}$$

3. The equation of continuity for an incompressible liquid simply states that mass in equals to mass out:

$$\frac{\partial u}{\partial x} + \frac{\partial v}{\partial y} + \frac{\partial w}{\partial z} = 0$$

4. Assuming that the coating fluid is Newtonian, i.e., its viscosity is constant, then Navier-Stokes equations will have the form:

$$\rho \left(u \frac{\partial u}{\partial x} + v \frac{\partial u}{\partial y} + w \frac{\partial u}{\partial z} + \frac{\partial u}{\partial t} \right) = \rho g_x - \frac{\partial P}{\partial x} + \mu \left(\frac{\partial^2 u}{\partial x^2} + \frac{\partial^2 u}{\partial y^2} + \frac{\partial^2 u}{\partial z^2} \right)$$

$$\rho \left(u \frac{\partial v}{\partial x} + v \frac{\partial v}{\partial y} + w \frac{\partial v}{\partial z} + \frac{\partial v}{\partial t} \right) = \rho g_y - \frac{\partial P}{\partial y} + \mu \left(\frac{\partial^2 v}{\partial x^2} + \frac{\partial^2 v}{\partial y^2} + \frac{\partial^2 v}{\partial z^2} \right)$$

$$\rho \left(u \frac{\partial w}{\partial x} + v \frac{\partial w}{\partial y} + w \frac{\partial w}{\partial z} + \frac{\partial w}{\partial t} \right) = \rho g_z - \frac{\partial P}{\partial z} + \mu \left(\frac{\partial^2 w}{\partial x^2} + \frac{\partial^2 w}{\partial y^2} + \frac{\partial^2 w}{\partial z^2} \right)$$

where μ is the viscosity of the coating color.

According to lubrication theory, the flow of coating material through the blade nip can be assumed as a two-dimensional laminar flow between converging or diverging walls. The flow is two dimensional because of asymmetry along the width of the blade. To maintain such a flow, the velocity component along the y and z directions must

be equal to zero: $v = 0$, $w = 0$. Also, all partial derivatives with respect to z vanish. Then equation of continuity reduced to:

$$\frac{\partial u}{\partial x} = 0$$

and the Navier-Stokes equations, assuming that gravitational forces are negligible, reduce to:

$$\rho \frac{\partial u}{\partial t} = -\frac{\partial P}{\partial x} + \mu \frac{\partial^2 u}{\partial y^2},$$

$$0 = -\frac{\partial P}{\partial y},$$

$$0 = -\frac{\partial P}{\partial z}.$$

So that pressure is a function of x and t . Also, for steady state flow conditions, the following is true:

$$0 = \frac{\partial u}{\partial t}$$

Finally, the Navier-Stokes equations are simplified to:

$$\frac{d^2u}{dy^2} = \frac{1}{\mu} \frac{dP}{dx}$$

This is the corresponding equation derived according to lubrication theory. Integrating this equation twice with respect to y yields:

$$u = \frac{1}{\mu} \frac{dP}{dx} \frac{y^2}{2} + Ay + B$$

Where A and B are arbitrary constants to be determined from the boundary conditions. The boundary conditions are obtained by considering that one boundary, the blade, is at rest and the other boundary, the web, is in motion at a constant velocity U , the speed of coating machine. So;

$$\text{at } y = 0 \text{ then } u = 0$$

$$\text{at } y = h(x) \text{ then } u = V$$

After this point, the corresponding equation is derived depending on whether the channel between substrate and the blade is assumed converging or parallel.

a) If it is a converging channel, the height of the gap will be a function of x and the equation will be:

$$V(x) = \left(\frac{V}{h(x)}\right)y - \left(\frac{dP}{dx} * \frac{h(x) y - y^2}{2\mu}\right)$$

b) If it is a parallel channel then the height (h_o) of the gab will be constant, as shown in Turai's equation below:

$$V = \left(\frac{V}{h_o}\right)y - \left(\frac{dP}{dx} * \frac{h_o y - y^2}{2\mu}\right)$$

Turai derived the final equation to calculate the hydrodynamic force underneath the blade as shown below:

$$F_{hy} = \frac{6\mu s^2 V}{h_o^2} \left(1 - \frac{2h_w}{h_o}\right)$$

where s = the length of bevelled surface,

h = the coating thickness experiencing shear,

h_w = the thickness of the wet coating,

μ = coating color viscosity,

V = web speed.

Appendix B

Determination of the Total Mass Flow Rate at Different Web Speeds

In blade coating process, as fluid is entering the blade region, not all of it can go through. Some fluid will go underneath the blade (R_2) driven by the pressure buildup upstream, and another part will be deflected away (R_1). The summation of these two components (R_1 and R_2) is equal to the total mass flow rate.

The total mass flow rate was determined in two steps. First the mass flow rate of excess coating color (R_1) was determined, later the mass flow rate of coating passing underneath the blade (R_2) was calculated from the coat weight of paper. In order to determine the total mass flow rate at each web speed (i.e., 600, 800, and 1000 fpm), the pilot-plant coater was run at constant blade tube pressure of 30 psi. Then, coated paper was saved to determine the mass flow rate passing underneath the blade while the R_1 was measured directly during the course of the run. The procedures to determine R_1 and R_2 are described below separately.

a) Determination of R_1

The excess amount of coating striking the blade was experimentally determined at each web speed. This was achieved by collecting the excess coating fluid (R_1) just after the coating color stroked the blade. The collecting of coating fluid was managed by attaching a collecting pipe below the blade nip at the underside of the blade, as

shown in Figure 11. The basic procedure was:

1. First, the collecting pipe was mounted to the coater.

2. Second, coating operation was started and both web speed and blade pressure was adjusted. While the pilot-plant coater was run at three different web speeds (i.e., 600, 800, and 1000 fpm), the blade pressure was constant at 30 psi at each speed.

3. Next, coater was run until the system reached steady state (about 3 min.).

4. Then, the excess amount of coating was collected in a container during 60 second time intervals.

5. Finally, the mass flow rate of excess coating color was calculated by dividing the total amount of coating collected into the container to the time interval. This procedure was repeated three times for each web speed. The purpose was to minimize the error due to any deviations in the mass flow rate of coating color. As a result, the average flow rate of excess coating color was calculated as shown in Table 19.

b. Determination of R_2

While the mass flow rate of excess coating color was measured, the coated paper was saved at each web speed in order to determine the mass flow rate passing underneath the blade (R_2). The coat weight of paper was calculated

Table 19
Mass Flow Rate of the Excess
Coating Color

Web Speed (fpm)	600	800	1000
$(R_1)_{\text{First}}$ (g/s)	449	515	701
$(R_1)_{\text{Second}}$ (g/s)	441	511	706
$(R_1)_{\text{Third}}$ (g/s)	444	514	702
Average (g/s)	445	513	703

by subtracting the weight of coated paper from the weight of the base sheet. The basis weight was determined according to the following procedure:

1. First, twenty base sheet samples were selected randomly from different part of the coating basestock. The diameter of each sample was 15.3 cm.

2. Second, the area of each sample was calculated (183.8 cm_2), then a conversion factor (54.39) was determined to calculate the basis weight in terms of g/m^2 as shown below:

$$\text{Area} = \frac{\pi D^2}{4} = 183.3 \text{ cm}^2$$

$$\frac{\text{Weight}(g)}{183.3 \text{ cm}^2} * \left(\frac{100 \text{ cm}}{1 \text{ m}}\right)^2 = (g) * 54.39 = \frac{g}{\text{m}^2}$$

3. Finally, each sample was weighted and basis weight was calculated by multiplying the weight of each circle with the conversion factor (54.39). The basis weight data were presented in Table 20. The same procedure was used to determine the weight of coated paper samples. Then, the coat weight was calculated by subtracting the weight of coated paper from the basis weight. Data to determine the coat weight at each web speed are presented in Tables 21-23. Three sets of data were collected to determine the mass flow rate of both excess coating (R_1) and the coating passing underneath the blade (R_2). Therefore, the average coat weight at each web speed is reported by taking the arithmetic average of the three sets of data as shown in Table 24. The wet coat weight at each web speed was calculated by dividing the dry coat weight to the solid percent of the coating color as shown below:

$$WCW = \frac{DCW}{\text{solid \%}}$$

where WCW = wet coat weight,

DCW = dry coat weight.

As a result, wet coat weight was calculated at each web speed, as shown in Table 25.

Table 20

Data for the Determination of Basis Weight

Weight of Each Sample (g)	Basis Weight (g/m ²)
1.71	92.76
1.69	92.12
1.70	92.55
1.70	92.22
1.69	91.93
1.71	92.70
1.70	92.53
1.70	92.34
1.70	93.04
1.70	92.62
1.71	92.50
1.70	92.53
1.69	92.55
1.70	92.54
1.71	93.02
1.70	92.53
1.70	92.52
1.69	92.53
1.69	91.90

Average = 92.17 g/m²

Table 21

Determination of Coat Weight
at 600 fpm and 30 psi

First Set of Data

Weight (g/cm ²)	Coated Weight (g/m ²)	Basis Weight (g/m ²)	Coat Weight (g/m ²)
1.793	97.528	92.17	5.36
1.799	97.855	92.17	5.69
1.781	96.876	92.17	4.71
1.805	98.159	92.17	5.99
1.789	97.316	92.17	5.15
1.793	97.523	92.17	5.35
1.778	97.707	92.17	4.54
1.781	96.897	92.17	4.73
1.761	95.809	92.17	3.64
1.762	95.853	92.17	3.69

Average = 4.88

Table 21--Continued

Second Set of Data

Weight (g/cm ²)	Coated Weight (g/m ²)	Basis Weight (g/m ²)	Coat Weight (g/m ²)
1.784	97.060	92.17	4.89
1.795	97.642	92.17	5.47
1.775	96.587	92.17	4.42
1.781	96.875	92.17	4.71
1.783	96.984	92.17	4.82
1.775	96.549	92.17	4.38
1.778	96.049	92.17	3.88
1.766	96.805	92.17	4.64
1.779	96.848	92.17	4.68
1.780	97.191	92.17	5.02

Average = 4.69

Table 21--Continued

Third Set of Data

Weight (g/cm ²)	Coated Weight (g/m ²)	Basis Weight (g/m ²)	Coat Weight (g/m ²)
1.783	96.989	92.17	4.82
1.793	97.533	92.17	5.36
1.781	96.880	92.17	4.71
1.784	97.044	92.17	4.87
1.786	97.152	92.17	4.98
1.791	97.424	92.17	5.25
1.782	96.935	92.17	4.76
1.781	96.880	92.17	4.71
1.779	96.848	92.17	4.68
1.780	97.191	92.17	5.02

Average = 4.92

Table 22

Determination of Coat Weight
at 800 fpm and 30 psi

First Set of Data

Weight (g/cm ²)	Coated Weight (g/m ²)	Basis Weight (g/m ²)	Coat Weight (g/m ²)
1.781	96.897	92.17	4.73
1.779	96.788	92.17	4.62
1.814	98.692	92.17	6.52
1.791	97.425	92.17	5.26
1.783	97.011	92.17	4.84
1.817	98.877	92.17	6.71
1.776	96.647	92.17	6.48
1.808	98.344	92.17	6.18
1.776	96.631	92.17	4.46
1.789	96.343	92.17	5.17
1.774	96.516	92.17	4.35

Average = 5.21

Table 22--Continued

Second Set of Data

Weight (g/cm ²)	Coated Weight (g/m ²)	Basis Weight (g/m ²)	Coat Weight (g/m ²)
1.777	96.701	92.17	4.53
1.779	96.767	92.17	4.60
1.824	99.241	92.17	7.07
1.811	98.529	92.17	6.36
1.799	97.865	92.17	5.70
1.810	98.458	92.17	6.29
1.784	97.077	92.17	4.91
1.791	97.463	92.17	5.29
1.778	96.729	92.17	4.56
1.785	97.131	92.17	4.96

Average = 5.43

Table 22--Continued

Third Set of Data

Weight (g/cm ²)	Coated Weight (g/m ²)	Basis Weight (g/m ²)	Coat Weight (g/m ²)
1.785	97.136	92.17	4.96
1.779	96.810	92.17	4.64
1.793	97.572	92.17	5.40
1.796	97.735	92.17	5.56
1.787	97.245	92.17	5.07
1.788	97.300	92.17	5.13
1.803	98.116	92.17	5.94
1.800	97.953	92.17	5.78
1.792	97.517	92.17	5.34
1.795	97.681	92.17	5.51

Average = 5.33

Table 23

Determination of Coat Weight
at 1000 fpm and 30 psi

First Set of Data

Weight (g/cm ²)	Coated Weight (g/m ²)	Basis Weight (g/m ²)	Coat Weight (g/m ²)
1.800	97.914	92.17	5.75
1.816	98.779	92.17	6.61
1.818	98.888	92.17	6.72
1.812	98.561	92.17	6.39
1.802	98.028	92.17	5.86
1.799	97.898	92.17	5.73
1.796	97.724	92.17	5.56
1.797	97.778	92.17	5.61
1.797	97.778	92.17	5.61
1.803	98.072	92.17	5.90

Average = 5.97

Table 23--Continued

Second Set of Data

Weight (g/cm ²)	Coated Weight (g/m ²)	Basis Weight (g/m ²)	Coat Weight (g/m ²)
1.805	98.203	92.17	6.04
1.802	98.018	92.17	5.85
1.795	97.675	92.17	5.51
1.804	98.143	92.17	5.98
1.810	98.480	92.17	6.32
1.813	98.643	92.17	6.48
1.792	97.501	92.17	5.34
1.794	97.604	92.17	5.44
1.798	97.838	92.17	5.67
1.791	97.419	92.17	5.26

Average = 5.79

Table 23--Continued

Third Set of Data

Weight (g/cm ²)	Coated Weight (g/m ²)	Basis Weight (g/m ²)	Coat Weight (g/m ²)
1.805	98.225	92.17	6.05
1.798	97.844	92.17	5.67
1.792	97.517	92.17	5.35
1.796	97.735	92.17	5.56
1.805	98.225	92.17	6.05
1.800	97.953	92.17	5.78
1.803	98.116	92.17	5.95
1.799	97.898	92.17	5.73
1.802	98.061	92.17	5.89
1.798	97.844	92.17	5.67

Average = 5.76

Table 24
Determination R_2 at Each Web Speed

	600 (fpm)	800 (fpm)	1000 (fpm)
Coat Weight at First Set	4.88 (g/m ²)	5.21 (g/m ²)	5.97 (g/m ²)
Coat Weight at Second Set	4.69 (g/m ²)	5.43 (g/m ²)	5.79 (g/m ²)
Coat Weight at Third Set	4.92 (g/m ²)	5.33 (g/m ²)	5.76 (g/m ²)
Average	4.83 (g/m ²)	5.32 (g/m ²)	5.84 (g/m ²)

Table 25
Determination of Wet Coat Weight

	Solid %	DCW (g/m ²)	WCW (g/m ²)
600 fpm	62.2	4.83	7.76
800 fpm	62.6	5.32	8.55
1000 fpm	62.9	5.84	9.28

Since both the web speed and the width of the coating flow were known, the flow rate passing underneath the blade could be calculated.

Sample Calculations at 600 fpm

When the web speed is 600 fpm (3.05 m/s), 3.05 m paper passes underneath the blade every second. The width of the coating flow is known (18 inches or 0.457 m), one can easily calculate the square meters of paper passing underneath the blade by multiplying the web speed with the

width of coating flow as shown below:

$$3.05 \frac{m}{s} * 0.457 m = 1.394 \frac{m^2}{s}$$

The mass flow rate passing underneath the blade can be calculated by multiplying this value with the wet coat weight as shown below:

$$1.394 \frac{m^2}{s} * 7.76 \frac{g}{m^2} = 10.8 \frac{g}{s}$$

As a result, the mass flow rate of the coating fluid passing underneath the blade was calculated. Overall results showing R_1 , R_2 , and the summation of them are presented in Table 26.

Table 26

Mass Flow Rates at Different Web Speeds

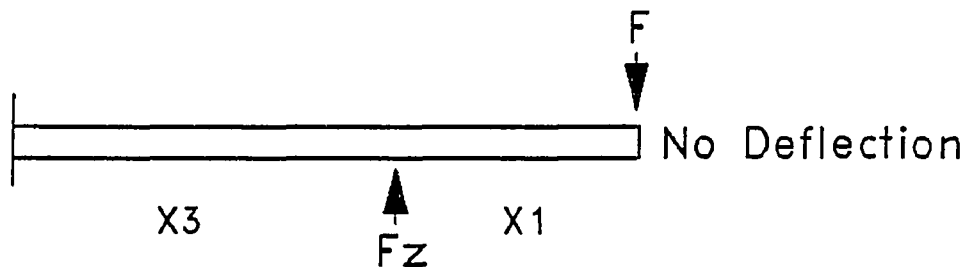
Speed (fpm)	% Solid	R_1 (g/s)	R_2 (g/s)	$m=R_1+R_2$ (kg/s)
600	62.2	443	10.8	0.45
800	62.7	513	15.6	0.53
1000	62.9	704	21.0	0.73

Appendix C

Derivation of the Corresponding Equation to
Transfer the Tube Pressure at the Tip of the Blade

In order to derive the corresponding equation to transfer the blade tube pressure to the tip of the blade, the blade deflection was assumed zero. This is valid when the net resultant force acting on the blade is zero.

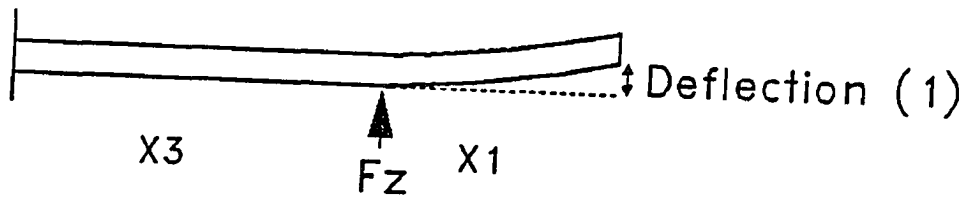
In this study, $(TDF)_{exp.}$ was determined under the conditions when it was almost equal to the blade tube pressure. When these two opposite forces become equal to each other, blade tube pressure and TDF will cancel each other. As a result, blade will stay straight as if there is no forces acting on the blade as illustrated below:



where $F_z =$ blade tube pressure.

The exact value of the blade tube pressure at the tip of the blade needs to be calculated because the $(TDF)_{exp.}$ was determine in terms of the blade tube pressure. The corresponding equation was derived in two steps:

1. First, the blade deflection arising only from the tube pressure was determined and it was called deflection 1, as shown below:



$$\delta = \frac{F_z * X_3^2 * (3X_3 + 3X_1 - X_3)}{6 * E * I} = \text{Deflection(1)}$$

where L_1 and L_2 = Blade dimensions

F_t = Tube pressure,

E = Elastic modules,

I = Moment of inertia,

2. Second, the blade deflection arising only from the TDF was investigated and called deflection 2, as shown below:



$$\delta = \frac{TDF * (X_3 + X_1)^3}{3 * E * I} = \text{Deflection(2)}$$

The magnitude of the hypothetical deflections arising from these blade tube pressure and TDF should counteract each other because these two forces are opposite but have the same magnitude. Therefore by equating these two deflection equations, TDF can be calculated as a function of blade tube pressure, as shown below:

$$\delta = \frac{F_z * X_3^2 * (3X_3 + 3X_1 - X_3)}{6 * E * I} = \frac{TDF * (X_3 + X_1)^3}{3 * E * I}$$

$$TDF = F = \frac{1}{2} * F_z * \frac{X_3^2 (3X_1 + 2X_3)}{(X_1 + X_3)^3}$$

This relationship was used to translate blade tube pressure to the force acting at the tip of the blade. The desired component of the tube pressure at the tip of the blade was calculated (Table 7) by multiplying with $\cos\alpha$.

$$TDF = F = \left[\frac{1}{2} * F_z * \frac{X_3^2 (3X_1 + 2X_3)}{(X_1 + X_3)^3} \right] * \cos\alpha$$

Appendix D
Coating Color Formulation

The coating formula consisting of No.1 clay, SB latex and CMC was prepared at 62 % solid. The following steps were followed in order to have a well dispersed coating formulation.

1. First, 70 % No.1 clay solution was prepared and mixed about 40 minutes.
2. Second, the dilution water was added to reduce the solid percentage up to 62 and solution was mixed 10 more minutes.
3. Next, latex was added and mixed 15 minutes.
4. Finally, CMC and dispersant were added gradually and the whole solution was mixed 10 minutes.

Table 27
Formulation

	Parts 100 Parts Pigments	% Solid	Wet Weight
Clay #1	100	100	100
Latex	10	48	20.8
CMC	0.15	25	0.6
Dispersant	0.013	15	0.09

Dry Weight = 110.16

Wet Weight = 121.5

Calculations were done on the base of 350 lb dry clay # 1.

Basis : 350 lb clay

$110.16 * 3.5 = 385.5$ lb total dry weight

$121.35 * 3.5 = 425.25$ lb total wet weight

$$\% \text{ Solid} = \frac{385.51}{425.25} * 100 = 90.7$$

Since 62 % solid was desired, some water was added to the mixing tank to reduce the solid % from 90.7 to 62. In order to have a 62 % solid, the total wet weight should be;

$$\text{Total Wet Weight} = \frac{100}{62} * 385.5 = 621.8 \text{ lb.}$$

Therefore, the total amount of water added to the mixing tank was;

$$\text{Total H}_2\text{O added} = 621.8 - 425.25 = 196.3 \text{ lb}$$

Appendix E
Coat Weight Versus Web Speed

Table 28

Determination of Coat Weight
at 500 fpm and 25 psi

First Set of Data

Weight (g/cm ²)	Coated Weight (g/m ²)	Basis Weight (g/m ²)	Coat Weight (g/m ²)
1.83	99.4	92.17	7.23
1.84	99.9	92.17	7.73
1.84	100.0	92.17	7.83
1.83	99.3	92.17	7.13
1.84	100.0	92.17	7.83
1.81	98.5	92.17	6.33
1.84	100.1	92.17	7.93
1.82	99.0	92.17	6.83
1.82	99.0	92.17	6.83
1.83	99.5	92.17	7.33

Average = 7.30

Table 28--Continued

Second Set of Data

Weight (g/cm ²)	Coat Weight (g/m ²)	Basis Weight.. (g/m ²)	Coat Weight (g/m ²)
1.82	99.1	92.17	6.93
1.83	99.7	92.17	7.53
1.83	99.7	92.17	7.53
1.80	98.1	92.17	5.93
1.83	99.7	92.17	7.53
1.83	99.7	92.17	7.53
1.84	100.2	92.17	8.03
1.83	99.7	92.17	7.53
1.84	100.2	92.17	8.03
1.83	99.6	92.17	7.43

Average = 7.40

Table 29

Determination of Coat Weight
at 750 fpm and 25 psi

First Set of Data

Weight (g/cm ²)	Coated Weight (g/m ²)	Basis Weight (g/m ²)	Coat Weight (g/m ²)
1.85	100.6	92.17	8.43
1.86	101.1	92.17	8.93
1.88	102.3	92.17	10.53
1.83	99.7	92.17	7.53
1.84	99.9	92.17	7.73
1.86	101.3	92.17	9.13
1.85	100.6	92.17	8.43
1.83	99.6	92.17	7.43
1.85	100.6	92.17	8.43
1.85	100.7	92.17	8.53
1.85	100.3	92.17	8.13

Average = 9.32

Table 29--Continued

Second Set of Data

Weight (g/cm ²)	Coated Weight (g/m ²)	Basis Weight (g/m ²)	Coat Weight (g/m ²)
1.83	99.7	92.17	7.53
1.87	101.7	92.17	9.53
1.85	100.6	92.17	8.43
1.88	102.4	92.17	10.23
1.86	101.3	92.17	9.13
1.86	101.2	92.17	9.03
1.83	99.6	92.17	7.43
1.88	102.2	92.17	10.03
1.85	100.7	92.17	8.53
1.87	101.7	92.17	9.53

Average = 8.94

Table 30

Determination of Coat Weight
at 1000 fpm and 25 psi

First Set of Data

Weight (g/cm ²)	Coated Weight (g/m ²)	Basis Weight (g/m ²)	Coat Weight (g/m ²)
1.96	106.6	92.17	14.43
1.97	107.3	92.17	15.13
1.97	107.2	92.17	15.03
1.99	108.5	92.17	16.33
1.96	106.7	92.17	14.53
1.96	106.4	92.17	14.23
1.98	107.5	92.17	15.33
1.96	106.7	92.17	14.53
1.98	107.7	92.17	15.53
1.95	106.2	92.17	14.03

Average=14.91

Table 30--Continued

Second Set of Data

Weight (g/cm ²)	Coated Weight (g/m ²)	Basis Weight (g/m ²)	Coat Weight (g/m ²)
1.99	108.3	92.17	16.13
1.98	107.7	92.17	15.53
1.98	107.9	92.17	15.73
1.98	107.4	92.17	15.23
1.97	107.0	92.17	14.83
1.98	107.7	92.17	15.53
1.95	106.2	92.17	14.03
1.94	105.2	92.17	13.03
1.96	106.6	92.17	14.43
1.97	107.2	92.17	15.03

Average = 14.95

Table 31
Results

Web Speed	500 fpm	750 fpm	1000 fpm
Coat Weight First Set	7.30 (g/m ²)	9.32 (g/m ²)	14.91 (g/m ²)
Coat Weight Second Set	7.40 (g/m ²)	8.94 (g/m ²)	14.95 (g/m ²)
Coat Weight Average	7.35 (g/m ²)	9.13 (g/m ²)	14.93 (g/m ²)

Appendix F

**Coat Weight Versus Blade Pressure Data
For the Second Pilot-Plant Trial**

Table 32
Coat Weight versus Blade Pressure
AT 500 fpm

at 45 psi		at 42 psi	
Sample Weight (g/m ²)	Total Weight (g/m ²)	Sample Weight (g/m ²)	Total Weight (g/m ²)
1.75	95.18	1.75	95.26
1.74	94.82	1.77	96.51
1.75	94.97	1.77	96.29
1.74	94.64	1.78	96.86
1.75	95.30	1.75	95.41
1.73	94.10	1.77	96.09
1.76	95.83	1.75	95.22
1.76	95.72	1.76	95.96
1.75	95.22	1.75	94.99
1.76	95.82	1.76	95.62
Average : 95.16		Average : 95.82	
Variance : 0.28		Variance : 0.34	
Standard Deviation : 0.53		Standard Deviation : 0.59	
Confident Interval : 0.36		Confident Interval : 0.40	

Table 32--Continued

at 39 psi		at 30 psi	
Sample Weight (g/m ²)	Total Weight (g/m ²)	Sample Weight (g/m ²)	Total Weight (g/m ²)
1.78	96.64	1.82	98.91
1.77	96.23	1.84	100.14
1.78	96.55	1.82	99.00
1.78	97.02	1.85	100.69
1.77	96.35	1.81	98.41
1.76	95.63	1.81	98.68
1.76	95.73	1.82	98.98
1.80	97.85	1.84	100.24
1.79	97.56	1.81	98.46
1.78	96.58	1.83	99.29
Average : 96.61		Average : 99.28	
Variance : 0.46		Variance : 0.57	
Standard Deviation : 0.68		Standard Deviation : 0.76	
Confident Interval : 0.46		Confident Interval : 0.52	

Table 32--Continued

at 25 psi		at 20 psi	
Sample Weight (g/m ²)	Total Weight (g/m ²)	Sample Weight (g/m ²)	Total Weight (g/m ²)
1.87	101.45	1.93	105.16
1.85	100.80	1.95	106.25
1.85	100.39	1.92	104.56
1.83	99.65	1.93	104.91
1.82	99.13	1.94	105.45
1.83	99.33	1.94	105.64
1.84	99.83	1.95	106.10
1.85	100.60	1.95	105.82
1.84	100.24	1.92	104.58
1.81	98.46	1.93	105.00
Average : 99.99		Average : 105.35	
Variance : 0.70		Variance : 0.33	
Standard Deviation : 0.84		Standard Deviation : 0.57	
Confident Interval : 0.58		Confident Interval : 0.39	

Table 32--Continued

at 15 psi		at 10 psi	
Sample Weight (g/m ²)	Total Weight (g/m ²)	Sample Weight (g/m ²)	Total Weight (g/m ²)
2.04	110.90	2.63	143.06
2.04	111.15	2.61	142.21
2.04	111.22	2.68	145.87
2.01	109.39	2.69	146.19
2.05	111.62	2.65	144.21
2.05	111.42	2.66	144.76
2.05	111.70	2.68	145.65
2.05	111.62	2.67	145.02
2.02	109.80	2.61	142.00
2.01	109.58	2.62	142.27
Average : 110.84		Average : 144.12	
Variance : 0.73		Variance : 2.36	
Standard Deviation : 0.85		Standard Deviation : 1.54	
Confident Interval : 0.69		Confident Interval : 1.06	

Table 33
Coat Weight Versus Blade Tube Pressure
at 500 fpm

Blade Tube Pressure (psi)	Coat Weight (g/m ²)
45	2.53 ± 0.36
42	3.19 ± 0.40
39	3.99 ± 0.46
30	6.65 ± 0.52
25	7.36 ± 0.58
20	12.72 ± 0.39
15	18.21 ± 0.59
10	98.69 ± 2.42
5	51.49 ± 1.06

Table 34
Coat Weight Versus Blade Pressure
AT 750 fpm

at 45 psi		at 10 psi	
Sample Weight (g/m ²)	Total Weight (g/m ²)	Sample Weight (g/m ²)	Total Weight (g/m ²)
1.75	95.16	1.78	96.63
1.75	95.19	1.76	95.76
1.75	95.23	1.78	96.81
1.75	95.05	1.77	96.21
1.74	95.73	1.76	95.58
1.76	95.51	1.78	96.72
1.78	96.81	1.74	94.76
1.77	96.26	1.75	94.96
1.75	95.22	1.76	95.64
1.76	95.82	1.76	95.62
Average : 95.50		Average : 95.87	
Variance : 0.35		Variance : 0.46	
Standard Deviation : 0.59		Standard Deviation : 0.68	
confident Interval : 0.41		Confident Interval : 0.46	

Table 34--Continued

at 39 psi		at 30 psi	
Sample Weight (g/m ²)	Total Weight (g/m ²)	Sample Weight (g/m ²)	Total Weight (g/m ²)
1.79	97.26	1.82	98.91
1.77	96.20	1.81	98.18
1.75	95.24	1.82	98.99
1.79	97.24	1.83	99.56
1.79	97.43	1.80	97.69
1.80	97.91	1.82	98.89
1.78	96.57	1.83	99.54
1.79	97.15	1.80	98.13
1.78	96.57	1.79	97.61
1.78	97.01	1.81	98.45
Average : 96.86		Average : 98.60	
Variance : 0.51		Variance : 0.44	
Standard Deviation : 0.71		Standard Deviation : 0.66	
Confident Interval : 0.49		Confident Interval : 0.45	

Table 34--Continue

at 25 psi		at 20 psi	
Sample Weight (g/m ²)	Total Weight (g/m ²)	Sample Weight (g/m ²)	Total Weight (g/m ²)
1.84	100.14	2.10	114.10
1.86	101.05	2.05	111.50
1.84	100.13	2.06	112.05
1.84	100.24	2.08	113.29
1.81	98.5	2.04	111.21
1.85	100.87	2.08	1113.21
1.84	100.15	2.09	113.57
1.85	100.39	2.08	113.13
1.83	99.39	2.07	112.40
1.84	100.30	2.07	112.83
Average : 100.12		Average : 112.73	
Variance : 0.47		Variance : 0.77	
Standard Deviation : 0.68		Standard Deviation : 0.88	
Confident Interval : 0.47		Confident Interval : 0.60	

Table 34--Continued

at 15 psi		at 10 psi	
Sample Weight (g/m ²)	Total Weight (g/m ²)	Sample Weight (g/m ²)	Total Weight (g/m ²)
2.52	137.32	2.79	151.74
2.47	134.53	2.86	155.79
2.41	131.08	2.77	150.39
2.42	131.47	2.79	151.75
2.45	133.19	2.76	150.18
2.42	131.39	2.82	153.45
2.41	131.15	2.85	155.14
2.47	134.35	2.75	149.58
2.49	135.28	2.76	150.24
2.45	133.41	2.78	151.11
Average : 133.32		Average : 151.94	
Variance : 3.93		Variance : 4.20	
Standard Deviation : 1.98		Standard Deviation : 2.05	
Confident Interval : 1.36		Confident Interval : 1.41	

Table 35

Coat Weight Versus Blade Tube Pressure
at 750 fpm

Blade Tube Pressure (psi)	Coat Weight (g/m ²)
45	2.87 ± 0.41
42	3.24 ± 0.46
39	4.23 ± 0.49
30	5.99 ± 0.45
25	7.49 ± 0.47
20	20.09 ± 0.60
15	18.21 ± 1.36
10	63.58 ± 1.41

Table 36
Coat Weight Versus Blade Pressure
At 1000 fpm

at 42 psi		at 39 psi	
Sample Weight (g/m ²)	Total Weight (g/m ²)	Sample Weight (g/m ²)	Total Weight (g/m ²)
1.75	95.27	1.78	97.03
1.76	95.68	1.78	97.01
1.78	96.71	1.77	96.28
1.76	95.58	1.78	96.91
1.77	96.14	1.78	96.99
1.76	95.53	1.80	97.77
1.78	96.79	1.78	96.86
1.77	96.21	1.80	97.95
1.75	95.22	1.79	97.42
1.79	97.10	1.77	96.31
Average : 96.02		Average : 97.05	
Variance : 0.41		Variance : 0.27	
Standard Deviation : 0.64		Standard Deviation : 0.52	
Confident Interval : 0.44		Confident Interval : 0.36	

Table 36--Continued

At 30 psi		at 25 psi	
Sample Weight (g/m ²)	Total Weight (g/m ²)	Sample Weight (g/m ²)	Total Weight (g/m ²)
1.83	99.77	1.84	100.28
1.81	98.45	1.83	99.55
1.80	98.09	1.85	100.74
1.80	98.11	1.83	99.44
1.82	98.74	1.83	99.39
1.82	99.1	1.86	100.90
1.80	98.02	1.87	101.96
1.82	99.05	1.83	99.60
1.81	98.35	1.85	100.72
1.83	99.40	1.84	100.14
Average : 98.72		Average : 100.27	
Variance : 0.34		Variance : 0.61	
Standard Deviation : 0.58		Standard Deviation : 0.78	
Confident Interval : 0.40		Confident Interval : 0.78	

Table 36--Continued

at 20 psi		at 15 psi	
Sample Weight (g/m ²)	Total Weight (g/m ²)	Sample Weight (g/m ²)	Total Weight (g/m ²)
2.15	116.67	3.25	176.83
2.17	117.97	3.24	176.44
2.24	122.10	3.38	183.60
2.16	117.48	3.31	180.28
2.10	114.29	3.38	184.02
2.16	117.48	3.24	176.06
2.12	115.06	3.23	175.92
2.19	119.37	3.21	174.65
2.15	116.87	3.37	183.54
2.10	114.09	3.37	183.29
Average : 117.14		Average : 179.46	
Variance : 5.26		Variance : 13.31	
Standard Deviation : 2.29		Standard Deviation : 3.65	
Confident Interval : 1.58		Confident Interval : 2.51	

Table 37

Coat Weight Versus Blade Tube Pressure
at 1000 fpm

Blade Tube Pressure (psi)	Coat Weight (g/m ²)
45	3.24 ± 0.41
42	3.39 ± 0.44
39	4.43 ± 0.36
30	6.09 ± 0.40
25	7.64 ± 0.78
20	24.52 ± 1.58
15	86.84 ± 2.51

Appendix G

Coat Weight Versus Blade Pressure Data for the Third Pilot-Plant Trial

Table 38
Coat Weight Versus Blade Pressure
at 600 fpm

at 22 psi		at 17 psi	
Sample Weight (g/m ²)	Total Weight (g/m ²)	Sample Weight (g/m ²)	Total Weight (g/m ²)
1.81	98.64	1.87	101.59
1.83	99.52	1.86	101.22
1.82	98.94	1.87	101.35
1.83	99.63	1.85	100.49
1.83	99.37	1.86	101.40
1.81	98.27	1.89	102.72
1.82	98.96	1.88	102.06
1.83	99.65	1.87	101.46
1.81	98.51	1.88	101.55
1.82	99.18	1.88	102.14
Average : 99.07		Average : 101.66	
Variance : 0.21		Variance : 0.33	
Standard Deviation : 0.46		Standard Deviation : 0.57	
Confident Interval : 0.32		Confident Interval : 0.39	

Table 38--Continued

at 15 psi		at 13 psi	
Sample Weight (g/m ²)	Total Weight (g/m ²)	Sample Weight (g/m ²)	Total Weight (g/m ²)
1.91	104.08	1.98	107.69
1.92	104.44	1.97	107.05
1.92	104.51	1.94	105.25
1.93	104.89	1.94	105.77
1.91	104.12	1.95	106.13
1.93	105.03	1.97	107.36
1.90	103.51	1.98	107.44
1.93	104.91	1.98	107.69
1.92	104.27	1.99	108.24
1.90	103.39	1.97	106.88
Average : 104.31		Average : 106.95	
Variance : 0.29		Variance : 0.32	
Standard Deviation : 0.54		Standard Deviation : 0.90	
Confident Interval : 0.37		Confident Interval : 0.62	

Table 38--Continued

at 12 psi		at 11 psi	
Sample Weight (g/m ²)	Total Weight (g/m ²)	Sample Weight (g/m ²)	Total Weight (g/m ²)
1.99	108.13	2.07	112.67
1.97	107.05	2.11	114.61
1.94	105.25	2.20	119.63
1.99	108.32	2.16	117.22
1.99	108.12	2.15	117.05
1.97	107.36	2.11	114.84
1.98	107.44	2.08	113.30
2.00	108.53	2.13	115.98
2.00	108.62	2.16	117.23
1.96	106.86	2.10	114.28
Average : 157.57		Average : 115.68	
Variance : 0.94		Variance : 4.09	
Standard Deviation : 0.97		Standard Deviation : 2.02	
Confident Interval : 0.67		Confident Interval : 1.39	

Table 38--Continued

at 10 psi		at 9 psi	
Sample Weight (g/m ²)	Total Weight (g/m ²)	Sample Weight (g/m ²)	Total Weight (g/m ²)
2.24	122.06	2.65	143.95
2.31	125.46	2.68	145.77
2.37	128.84	2.85	155.01
2.42	131.45	2.76	150.12
2.33	126.55	2.65	144.14
2.27	123.43	2.65	144.14
2.28	123.77	2.55	138.70
2.45	132.99	2.65	144.14
2.33	126.90	2.66	144.55
2.30	125.18	2.70	146.86
Average : 126.66		Average : 145.74	
Variance : 11.14		Variance : 16.84	
Standard Deviation : 3.34		Standard Deviation : 4.10	
Confident Interval : 2.29		Confident Interval : 2.82	

Table 39

Coat Weight Versus Blade Tube Pressure
at 600 fpm

Blade Tube Pressure (psi)	Coat Weight (g/m ²)
22	6.90 ± 0.32
17	9.50 ± 0.39
15	12.1 ± 0.37
13	14.8 ± 0.62
12	15.4 ± 0.67
11	23.5 ± 1.39
10	34.5 ± 2.29
9	99.2 ± 2.82

Table 40
Coat Weight Versus Blade Pressure
At 800 fpm

at 25 psi		at 20 psi	
Sample Weight (g/m ²)	Total Weight (g/m ²)	Sample Weight (g/m ²)	Total Weight (g/m ²)
1.83	99.72	1.87	101.52
1.82	99.06	1.90	103.19
1.83	99.60	1.86	101.23
1.83	99.29	1.87	101.58
1.82	99.16	1.86	101.41
1.84	99.85	1.86	101.25
1.83	99.31	1.87	101.64
1.82	99.06	1.89	102.66
1.84	100.04	1.89	102.63
1.83	99.65	1.89	102.92
Average : 99.47		Average : 102.00	
Variance : 0.11		Variance : 0.51	
Standard Deviation : 0.34		Standard Deviation : 0.72	
Confident Interval : 0.22		Confident Interval : 0.49	

Table 40--Continued

At 18 psi		at 17 psi	
Sample Weight (g/m ²)	Total Weight (g/m ²)	Sample Weight (g/m ²)	Total Weight (g/m ²)
1.89	102.62	1.92	104.39
1.90	103.07	1.90	103.50
1.90	103.08	1.91	103.90
1.90	103.40	1.93	105.22
1.88	102.26	1.91	103.92
1.87	101.90	1.93	104.79
1.90	103.60	1.93	104.71
1.89	102.85	1.92	104.31
1.88	102.50	1.93	104.99
1.88	102.38	1.94	105.49
Average : 102.77		Average : 104.52	
Variance : 0.26		Variance : 0.36	
Standard Deviation : 0.51		Standard Deviation : 0.60	
Confident Interval : 0.35		Confident Interval : 0.41	

Table 40--Continued

at 16 psi		at 15 psi	
Sample Weight (g/m ²)	Total Weight (g/m ²)	Sample Weight (g/m ²)	Total Weight (g/m ²)
2.27	123.47	2.75	149.58
2.26	122.92	2.69	146.31
2.29	124.56	2.63	143.05
2.31	125.89	2.72	148.02
2.27	123.47	2.81	152.84
2.30	125.10	2.67	145.12
2.25	122.38	2.72	147.94
2.35	128.06	2.88	156.65
2.39	129.82	2.72	147.78
2.41	131.08	2.75	149.80
Average : 125.67		Average : 148.71	
Variance : 8.19		Variance : 13.46	
Standard Deviation : 2.86		Standard Deviation : 3.67	
Confident Interval : 1.97		Confident Interval : 2.52	

Table 41
Coat Weight Versus Blade Tube Pressure
at 800 fpm

Blade Tube Pressure (psi)	Coat Weight (g/m ²)
25	7.30 ± 0.22
20	9.80 ± 0.49
18	10.6 ± 0.35
17	12.4 ± 0.41
16	33.5 ± 1.97
15	56.5 ± 2.52
14	84.12 ± 3.28

Table 42
Coat Weight Versus Blade Pressure
At 1000 fpm

at 35 psi		at 30 psi	
Sample Weight (g/m ²)	Total Weight (g/m ²)	Sample Weight (g/m ²)	Total Weight (g/m ²)
1.83	99.45	1.83	99.67
1.82	99.07	1.83	99.30
1.83	99.30	1.84	99.89
1.83	99.33	1.83	99.66
1.83	99.36	1.83	99.51
1.82	98.76	1.84	99.86
1.82	99.15	1.84	100.14
1.84	99.89	1.82	99.19
1.83	99.31	1.83	99.30
1.83	99.43	1.82	99.24
Average : 99.31		Average : 99.58	
Variance : 0.08		Variance : 0.09	
Standard Deviation : 0.28		Standard Deviation : 0.31	
Confident Interval : 0.19		Confident Interval : 0.21	

Table 42--Continued

at 28 psi		at 26 psi	
Sample Weight (g/m ²)	Total Weight (g/m ²)	Sample Weight (g/m ²)	Total Weight (g/m ²)
1.86	100.93	1.85	100.65
1.83	99.60	1.86	101.28
1.87	101.50	1.86	101.18
1.84	100.34	1.87	101.53
1.86	100.93	1.85	100.53
1.87	101.58	1.88	102.40
1.86	100.98	1.84	100.06
1.84	100.12	1.84	100.10
1.83	99.56	1.84	100.11
1.85	100.82	1.85	100.82
Average : 100.64		Average : 100.86	
Variance : 0.46		Variance : 0.50	
Standard Deviation : 0.68		Standard Deviation : 0.71	
Confident Interval : 0.46		Confident Interval : 0.49	

Table 42--Continued

at 25 psi		at 24 psi	
Sample Weight (g/m ²)	Total Weight (g/m ²)	Sample Weight (g/m ²)	Total Weight (g/m ²)
1.85	100.68	1.87	101.72
1.85	100.69	1.88	102.45
1.85	100.66	1.91	103.74
1.87	101.59	1.87	101.63
1.85	100.79	1.87	101.55
1.87	101.62	1.90	103.50
1.89	102.54	1.87	101.95
1.84	100.12	1.87	101.55
1.85	100.80	1.90	103.20
1.86	101.29	1.88	102.35
Average : 101.08		Average : 102.36	
Variance : 0.43		Variance : 0.63	
Standard Deviation : 0.66		Standard Deviation : 0.80	
Confident Interval : 0.45		Confident Interval : 0.55	

Table 42--Continued

at 23 psi		at 22 psi	
Sample Weight (g/m ²)	Total Weight (g/m ²)	Sample Weight (g/m ²)	Total Weight (g/m ²)
1.90	103.51	2.04	110.71
1.91	103.69	2.10	114.00
1.89	102.80	2.02	110.02
1.90	103.35	2.13	115.72
1.89	102.89	2.00	108.84
1.85	100.62	2.05	101.26
1.90	103.34	2.03	110.44
1.89	102.91	2.05	111.70
1.89	102.80	2.07	112.34
1.95	106.06	2.03	110.52
Average : 103.20		Average : 111.56	
Variance : 1.57		Variance : 3.69	
Standard Deviation : 1.25		Standard Deviation : 1.92	
Confident Interval : 0.86		Confident Interval : 1.32	

Table 43

Coat Weight Versus Blade Tube Pressure
at 1000 fpm

Blade Tube Pressure (psi)	Coat Weight (g/m ²)
35	7.10 ± 0.19
30	7.40 ± 0.21
28	8.50 ± 0.46
26	8.70 ± 0.49
25	8.90 ± 0.45
24	10.2 ± 0.55
23	11.0 ± 0.86
22	19.4 ± 1.32
21	48.7 ± 3.34

Appendix H
Determination of the Incoming Layer
Thickness

Sample Calculations for 600 fpm

$$m = V * D * S$$

where m = mass flow rate (kg/s),

V = web speed (m/s),

D = density of the coating color (kg/m³),

S = cross sectional area of incoming coating color (m²).

$$S = W * h_2$$

where W = width of the substrate (m),

h_2 = thickness of incoming coating layer (m).

$$h_2 (m) = \frac{m (kg/s)}{D (kg/m^3) * V (m/s) * W (m)}$$

$$h_2 = \frac{0.45 (kg/s)}{1523 (kg/m^3) * 3.07 (m/s) * 0.457 (m)} = 21.06 * 10^{-5} m$$

$$h_2 = 21.06 * 10^{-5} m * \left(\frac{1 * 10^6 \text{ } \mu m}{1 m} \right) = 210.6 \text{ } \mu m$$

Appendix I
Calculation of Hydrodynamic Force
Based on Lubrication Theory

Sample Calculations at 600 fpm

$$F_{hy} = \left[\frac{6\mu s^2 V}{h_o^2} \left(1 - \frac{2h_w}{h_o}\right) \right] * \cos\alpha$$

where s = the length of bevelled surface (610 μm),

h_o = the coating thickness experiencing shear (60 μm),

h_w = the thickness of the wet coating (22 μm),

μ = coating color viscosity (0.016 kg/m-s),

V = web speed (3.07 m/s).

$$s = \frac{\text{Thickness of the Blade}}{\sin\alpha} = \frac{400}{\sin 41} = 610 \text{ (}\mu\text{m)}$$

$$F_{hy} = \left[\frac{6 * 0.016 \text{ (kg/m-s)} * 610^2 \text{ (}\mu\text{m)}^2 * 3.07 \text{ (m/s)}}{60^2 \text{ (}\mu\text{m)}^2} * \left(1 - \frac{2 * 22 \text{ (}\mu\text{m)}}{60 \text{ (}\mu\text{m)}}\right) \right] \cos 41 = 6.13 \text{ (N/m)}$$

$$6.13 \left(\frac{\text{N}}{\text{m}}\right) * \left(\frac{1}{\text{s}}\right) = 6.13 \left(\frac{\text{N}}{\text{m}}\right) * \left(\frac{1}{610 * 10^{-6} \text{ m}}\right) = 1.00 * 10^4 \text{ (N/m}^2\text{)}$$

$$1.00 * 10^4 \text{ (Pa)} * \left(\frac{1 \text{ kPa}}{1000 \text{ Pa}} * \frac{1 \text{ atm}}{101.3 \text{ kPa}} * \frac{14.7 \text{ psia}}{1 \text{ atm}}\right) = 1.45 \text{ psia}$$

Appendix J
Calculation of the Dynamic Forces
Based on Impact Model

Sample Calculations at 600 fpm

Impulse Force

$$RZ = [m * V * \frac{(1 + \cos\alpha)}{\sin\alpha}] * \cos\alpha \quad [9]$$

where m = the mass flow rate (0.45 kg/s),

V = the velocity of the coating color or web speed
(3.07 m/s),

α = the blade bevel angle (41 degrees).

$$RZ = [0.45 \text{ (kg/s)} * 3.07 \text{ (m/s)} * \frac{(1 + \cos 41)}{\sin 41}] * \cos 41 = 2.788 \text{ (kg/m-s}^2\text{)}$$

$$P = \frac{\text{Force}}{\text{Area}} = \frac{F}{W_1 * 0.9h_2}$$

where W_1 = width of the blade (0.762 m or 30 inch)

h_2 = thickness of the incoming coating layer (m)

$$P = \frac{2.788 \text{ N}}{0.762 \text{ (m)} * 0.9 * 211 * 10^{-6} \text{ (m)}} = 1.93 * 10^4 \text{ (N/m}^2\text{)}$$

$$1.93 * 10^4 \text{ (Pa)} * \left(\frac{1 \text{ kPa}}{1000 \text{ Pa}}\right) * \left(\frac{1 \text{ atm}}{101.3 \text{ kPa}}\right) * \left(\frac{14.7 \text{ psia}}{1 \text{ atm}}\right) = 2.8 \text{ psia}$$

Pressure Force

$$P_z = \frac{1}{2} mV \frac{\pi}{\alpha} * [1 - (0.5 - \frac{1}{\pi}) * \frac{h_o}{h_2}] * [1 - \frac{1}{2 * \frac{\pi}{\alpha} - 1}] * [\frac{1}{1 - (0.5 - \frac{1}{\pi}) * \frac{h_o}{h_2}}]^2$$

where P_z = Pressure force (N),

m = Mass flow rate of coating color (0.45 kg/s),

V = Web speed (3.07 m/s),

α = Blade bevel angle (41 degrees),

h_o = the thickness of coating color passing under the blade tip (22 μm),

h_2 = the thickness of coating color reaching the blade (211 μm).

$$P_z = \frac{1}{2} 0.45 \text{ (kg/s)} * 3.07 \text{ (m/s)} \frac{180}{41} * [1 - (0.5 - \frac{1}{180}) * \frac{22 \text{ (}\mu\text{m)}}{211 \text{ (}\mu\text{m)}}]$$

$$[1 - \frac{1}{2 * \frac{180}{41} - 1}] * [\frac{1}{1 - (0.5 - \frac{1}{180}) * \frac{22 \text{ (}\mu\text{m)}}{211 \text{ (}\mu\text{m)}}}]^2] * \cos 41 = 2.1 \text{ N}$$

$$P = \frac{\text{Force}}{\text{Area}} = \frac{F}{W_1 * 0.9h_2}$$

where W_1 = width of the blade (0.762 m or 30 inch)

h_2 = thickness of the incoming coating layer (m)

$$P = \frac{2.1 \text{ N}}{0.762 \text{ (m)} * 0.9 * 211 * 10^{-6} \text{ (m)}} = 1.45 * 10^4 \text{ (N/m}^2\text{)}$$

$$1.45 * 10^4 \text{ (Pa)} * \left(\frac{1 \text{ kPa}}{1000 \text{ Pa}} \right) * \left(\frac{1 \text{ atm}}{101.3 \text{ kPa}} \right) * \left(\frac{14.7 \text{ psia}}{1 \text{ atm}} \right) = 2.1 \text{ psia}$$

Hydrodynamic Force to the Proximity of the Blade

$$H_z = \left(\frac{6\mu_1 V}{\tan^2 \alpha} * \left[\ln 1+r - \frac{2*r}{2+r} \right] \right) * \cos \alpha$$

where H_z = Hydrodynamic force (N)

V = Web speed (3.07 m/s)

μ = viscosity at proximity to the blade (0.012 kg/m-s),

h_1 = the thickness of coating color reaching the
blade (211 um),

$r = h_1/h_0 - 1. = 211/(22-1) = 10.05$

$$H_z = \left(\frac{6 * 0.012 \text{ (kg/m-s)} * 3.07 \text{ (m/s)}}{\tan^2 41} * \left[\ln 11 - \frac{2 * 10.05}{2 + 10.05} \right] \right) * \cos 41 = 0.21 \text{ N}$$

$$P = \frac{\text{Force}}{\text{Area}} = \frac{F}{W_1 * 0.9 h_2}$$

where W_1 = width of the blade (0.762 m or 30 inch)

h_2 = thickness of the incoming coating layer (m)

$$P = \frac{0.21 \text{ N}}{0.762 \text{ (m)} * 0.9 * 211 * 10^{-6} \text{ (m)}} = 1.48 * 10^3 \text{ (N/m}^2\text{)}$$

$$1.48 * 10^3 \text{ (Pa)} * \left(\frac{1 \text{ kPa}}{1000 \text{ Pa}} \right) * \left(\frac{1 \text{ atm}}{101.3 \text{ kPa}} \right) * \left(\frac{14.7 \text{ psia}}{1 \text{ atm}} \right) = 0.22 \text{ psia}$$

REFERENCES

1. Hartman, K.J., "The Market for Coated Paper", Tappi J. 69 (9) pp. 58-63 (Sep., 1986).
2. Kahila, S.J., and Eklund, D.E., "Factors Influencing the Coat Weight in Blade Coating with Bevelled Blade Theory and Practice," Tappi Coating Conference Proceedings, Atlanta, GA, TAPPI Press, 1978, pp. 13-29.
3. Turai, L.L., "Analysis of Blade Coating Process," Tappi J., 54 (8), pp. 1315-1318 (Aug., 1971).
4. Kuzmak, J.M., "Factors Affecting Coat Weight in Bevelled Blade Coating," Tappi Coating Conference Proceedings, Atlanta, GA, TAPPI Press, 1985, pp. 5-12.
5. Kartovaara, A. "Lateral Force under the Blade Tip in Bevelled Blade Coating," Tappi Coating Proceedings, pp. 385-399.
6. Franckh, F.R., and Scriven, L.E., "The Physics of Blade Coating on Deformable Substrate," Tappi Coating Conference Proceedings, Atlanta, GA, TAPPI Press, 1988, pp. 217-238.
7. Triantafillopoulos, N.G., and Farrington, T., "Flash X-Ray Radiograph Technique for Visualizing Coating Flows," Tappi Coating Conference Proceedings, Atlanta, GA, Tappi Press, 1988, pp. 42-52.
8. Follette, W.J., and Fowells, R.W., "Operating Variables of a Blade Coater," Tappi J., 43 (11), pp. 953-957 (Nov. 1960).
9. Denn, M.M., Process Fluid Mechanics, Prentice-Hall, Englewood Cliffs, N.J., 1980, pp. 333-334.
10. Bohmer, E., "The Relationship between Coat Weight and Other Variables During Blade Coating," Svensk Papperstiding, 67 (9), pp. 347-355 (May 15, 1964).
11. Clark, N.O., Windle, W., and Restall, C.A. Paper Trade J., 150 (38), pp. 49-54 (Jan., 1986).
12. Modrak, J.P., "Effect of Coating Rheology on the Blade

Coating Process," Tappi J., 56 (10), pp. 70-73 (Oct. 1973).

13. Hayward, G., "Factors Affecting the Metering Characteristics of a Blade Coater," Tappi Coating Conference Proceedings, Atlanta, GA, TAPPI Press, 1973, pp. 61-73.

14. Gartaganis, P.A., Cleland, A.J., and Wairegi, T., "Blade Mechanics of Extended Blade Coaters," Tappi J., 61 (4), pp. 77-81 (April 1978).

15. Hwang, S.S., "Hydrodynamic Analyses of Blade Coaters," Chem.Eng. Sci., 34 (2), pp. 181-189.

16. Eklund, D.E., "Influence of Blade Geometry and Blade Pressure on the Appearance of a Coated Surface," Tappi Coating Conference Proceedings, Atlanta, GA, TAPPI Press, 1981, pp. 49-57.

17. Ginn, R.F., "High Shear Rheology in Blade Coater," J. Pulp and Paper Sci., 109(4), pp. 89-98 (July 1984).

18. Guzy, C.J., and Higgins, B.G., "Viscous Pressure Across the Nip of a Blade Coater and its Effect on the Final Coated Film Thickness," Tappi Coating Conference Proceedings, Atlanta, GA, TAPPI Press, 1982: 63-71.

19. Windle, W., and Beazley, K.M., "The Mechanism of Blade Coating," Tappi J., 50 (1), pp. 1-7 (Jan., 1967).

20. Windle, W., and Beazley, K.M., "The Role of Viscoelasticity in Blade Coating," Tappi J., 51 (8), pp. 340-348 (Aug., 1968).

21. Sullivan, T., Middleman, S., and Keunings, R., "Use of a Finite Element Method to Interpret Rheological Effects in Blade Coating," AIChE J., 33(12), pp. 2047-2056 (Dec. 1987).

22. Chen, K.A.S., and Scriven, L.E., "On the Physics of Liquid Penetration into a Deformable Porous Substrate," Tappi Coating Conference Proceedings, Atlanta, GA, TAPPI Press, 1989, pp. 93-106.

23. Kuzmak, J.M., "Bevelled Blade Coating," Tappi J., 69 (2), pp.72-75 (Feb., 1986).

24. Huang, D.K., "Blade Streaks and Scratch Problem," Blade Coating Seminar, Atlanta, GA, TAPPI Press, 1986, pp. 175-186.

25. Bliesner, W.C., "Basic Mechanism in Blade Coating," Tappi J., 54 (10), pp. 1673-1679 (Oct., 1971).